CALCULATION OF THE RAMAN FREQUENCIES USING VOLUME DATA IN VARIOUS PHASES OF SOLID NITROGEN AND BENZENE

A THESIS SUBMITTED TO
THE GRADUATE SCHOOL OF NATURAL AND APPLIED SCIENCES
OF
MIDDLE EAST TECHNICAL UNIVERSITY

BY

ESİN ÇETİNBAŞ İŞERİ

IN PARTIAL FULFILLMENT OF THE REQUIREMENTS
FOR
THE DEGREE OF MASTER OF SCIENCE
IN
PHYSICS

SEPTEMBER 2011

Approval of the thesis:

CALCULATION OF THE RAMAN FREQUENCIES USING VOLUME DATA IN VARIOUS PHASES OF SOLID NITROGEN AND BENZENE

submitted by **ESİN ÇETİNBAŞ İŞERİ** in partial fulfillment of the requirements for the degree of **Master of Science in Physics Department, Middle East Technical University** by,

Prof. Dr. Canan Özgen _____
Dean, Graduate School of **Natural and Applied Sciences**

Prof. Dr.Sinan Bilikmen _____
Head of Department, **Physics**

Prof. Dr. Hamit Yurtseven _____
Supervisor, **Physics Department., METU**

Examining Committee Members:
Prof. Dr. Mehmet Parlak _____
Physics Dept., METU

Prof. Dr. Hamit Yurtseven _____
Physics Dept., METU

Assoc. Prof. Dr. Enver Bulur _____
Physics Dept., METU

Assoc. Prof., Dr. Barış Akoğlu _____
Physics Engineering Dept., Ankara University

Assist. Prof. Dr. Alpan Bek _____
Physics Dept., METU

Date: _____

I hereby declare that all information in this document has been obtained and presented in accordance with academic rules and ethical conduct. I also declare that, as required by these rules and conduct, I have fully cited and referenced all materials and results that are not original to this work.

Name, Last name: Esin Çetinbaş İşeri

Signature :

ABSTRACT

CALCULATION OF THE RAMAN FREQUENCIES USING VOLUME DATA IN VARIOUS PHASES OF SOLID NITROGEN AND BENZENE

Çetinbaş İşeri, Esin
M. Sc., Department of Physics
Supervisor: Prof. Dr. Hamit Yurtseven

September 2011, 57 pages

The temperature and pressure dependences of the Raman frequencies of some lattice and internal modes are calculated using the volume data from the literature through the mode Grüneisen parameters. This calculation is performed in different phases of solid nitrogen and benzene. Calculated Raman frequencies are compared with the experimentally measured frequencies for those crystalline systems studied.

Keywords: Raman frequency, solid nitrogen, benzene.

ÖZ

KATI AZOT VE BENZENIN ÇEŞİTLİ FAZLARINDA HACİM VERİSİ KULLANARAK RAMAN FREKANSLARININ HESAPLANMASI

Çetinbaş İşeri, Esin
Yüksek Lisans, Fizik Bölümü
Tez Yöneticisi: Prof. Dr. Hamit Yurtseven
Eylül 2011, 57 sayfa

Literatürden hacim verisi kullanarak, bazı örgü ve iç kiplerin Raman frekanslarının sıcaklık ve basınç bağlılığı kip Grünesien parametreleri aracılığıyla hesaplanmıştır. Bu hesaplama, katı azot ve benzenin değişik fazlarında gerçekleştirilmiştir. Hesaplanan Raman frekansları çalışılan bu kristalik sistemler için deneysel olarak ölçülen frekanslarla karşılaştırılmıştır.

Anahtar Kelimeler: Raman frekansı, katı azot, benzen.

ACKNOWLEDGEMENTS

I am sincerely and heartily grateful to my supervisor, Hamit Yurtseven, for the support and guidance he showed me throughout my thesis. I am sure it would have not been possible without his help.

I owe sincere and earnest thankfulness to my parents. They have given me their unequivocal support throughout, as always. Besides I would like to thank my dear husband, Erkut İnan İşeri, for supporting and encouraging me to pursue this degree.

TABLE OF CONTENTS

LIST OF TABLES

TABLES

LIST OF FIGURES

FIGURES

CHAPTER 1

INTRODUCTION

Critical phenomena and phase transitions is one of the main interests of physics. A brief summary of this topic is given in this chapter. The more detailed information can be obtained from the references [1-5].

1.1 Phase and Phase Transition

It is convenient to start our summary by defining phase. A phase is a state of matter in which the microscopic physical properties of the substance are uniform on a macroscopic length scale. A phase is characterized by a thermodynamic function, typically the free energy (Gibbs function) which is a function of a few macroscopic parameters such as temperature and pressure.

A substance under the suitable conditions of temperature and pressure exhibits three phases; solid, liquid and vapor. Thus, the phase of a macroscopic substance is determined by the values of the temperature and pressure parameters. In order to determine the circumstances under which any of these phases can co-exist, it is convenient to study the variation with temperature and pressure of the Gibbs function, G. Two phases of the same substance can only co-exist in equilibrium if they possess the same Gibbs function per unit mass.

A phase diagram is a graph with those parameters as the axes, on which the phase is specified for each point. A typical phase diagram (figure 1.1) has several specific features including phase boundaries, a critical point and a triple point. A phase boundary separates different phases. A change in parameters such as the

temperature across a phase boundary causes a sudden change in the phase of a substance. For example, a solid phase changes into a liquid phase at the melting temperature. This is a phase transition. A phase boundary sometimes disappears at a critical point, where two phases become indistinguishable and the substance shows anomalous behavior. The theory of critical phenomena explains this anomalous behavior. Three different phases coexist at the triple point.

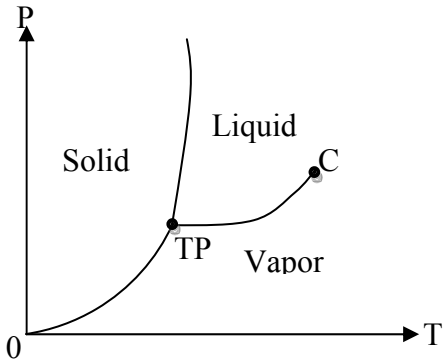

Figure 1.1 Typical phase diagram. The phase of a substance is determined by the values of the control parameters such as pressure P and temperature T. C denotes the critical point and TP stands for the triple point.

A phase can be characterized by various physical quantities. Especially important is the order parameter which measures how microscopic elements constituting the macroscopic phase are ordered or in a similar state. The order parameter is associated with the breaking of a symmetry of the system under consideration.

A phase transition is a phenomenon in which a drastic change between thermodynamic phases occurs as the system parameters such as the temperature and pressure varied. The characterization of a phase transition as a drastic change of macroscopic properties is described theoretically as the emergence of singularities (non-analyticities) in functions representing physical quantities such as free energy.

In the first order phase transition, first derivatives of thermodynamic potentials jump discontinuously and this implies a nonzero latent heat. The order

parameter also jumps discontinuously. The 'order' of a transition is determined by the lowest order of differential coefficient of the Gibbs function, G (free energy) which shows a discontinuity on the transition line. Thus, in a first order phase transition which involves latent heat, free energy is continuous across the line, but its derivatives are discontinuous. An example of this is the vaporization of a liquid to a gas, where the matter has to absorb a certain amount of energy which is the latent heat, in order to completely turn to another phase.

A phase transition is said to be of the second order when there does not exist a surface of discontinuity during the transition. One example of this is the ferromagnetic transition.

In the transition of a superconductor in zero magnetic field there is no latent heat and no volume change, so that the first derivatives of G are continuous, but the second derivatives, representing specific heat, expansion coefficient and compressibility are discontinuous, so that this is a transition of the second order.

1.2 Critical Phenomena

Second order phase transitions are often synonymous with critical phenomena, i.e. anomalous phenomena that appear around the critical point (C in fig. 1.1) where two or more phases become indistinguishable.

In figure 1.1, the transition lines between phases are called the coexistence lines. Crossing a coexistence line leads to a first order phase transition, which is characterized by a discontinuous change in some thermodynamic quantity such as volume, enthalpy, magnetization.

The solid - gaseous phases and the solid - liquid phases and liquid - gaseous phases are in equilibrium along the coexistence lines called the sublimation curve, the fusion curve, and the vapor pressure curve respectively (Fig. 1.1). Each point on these three curves represents an equilibrium state in which two or more phases

can coexist and the triple point (TP) represents an equilibrium state in which all three phases coexist.

Notice that, while the fusion curve, in principle, can be extended to infinity, the vapor pressure curve terminates at a point beyond which the two phases cannot be distinguished (Fig. 1.1). This point is called a critical point(C) and beyond the critical point, the system is in a supercritical fluid state. Termination of vapor pressure curve in a critical point means that a liquid can be converted to a gas continuously, without crossing the phase transition line at the critical point. The temperature at which this point occurs is called the critical temperature T_C.

At the critical temperature the compressibility decreases at first as the volume is reduced, and then rises to infinity at point C in fig. 1.1; further compression reduces the compressibility steadily. At temperatures well above Tc the compressibility decreases monotonically as the volume is reduced, so that although at large volumes the substance may be regarded as vapor-like, and at low volumes as liquid-like, there is no point at which any transition from one phase to another may be said to have occurred. It is therefore possible, by travelling around the point C in fig. 1.1, to make a transition from what is undoubtedly the vapor phase to the equally undoubted liquid phase, without any abrupt change in the properties of the system.

It is widely believed that there is not a critical point in the fusion curve between solid and liquid. If such a point existed it would be possible, by going around it, to make a continuous transition from the liquid to the solid phase. Since the properties of normal liquids are strictly isotropic, they possess no crystalline structure which singles out anyone direction as different from another, while true solids (excluding glasses and similar amorphous phases) possess non-spherical symmetries which are characteristic of the regular arrangement of their molecules in a crystalline lattice. In order to go from the liquid to the crystalline phase, therefore, it is necessary to make a change of the symmetry properties, and this is of necessity a discontinuous process. The symmetry properties of a lattice are describable in terms of certain geometrical operations, such as translation or

reflexion, which displace every atom on to another identical atom and so leave the lattice unaltered. A given phase either possesses or does not possess any given symmetry property, and thus no continuous transition is possible and no critical point can exist. However, thus far it has not been possible to prove the non-existence of a liquid-solid critical point.

At a critical point C (Fig. 1.1), thermodynamic quantities such as volume, enthalpy and magnetization remain continuous, but derivatives of these functions may diverge. Examples of such divergent quantities are the heat capacity, isothermal compressibility, magnetic susceptibility, etc. These divergences occur in a universal way for large classes of systems.

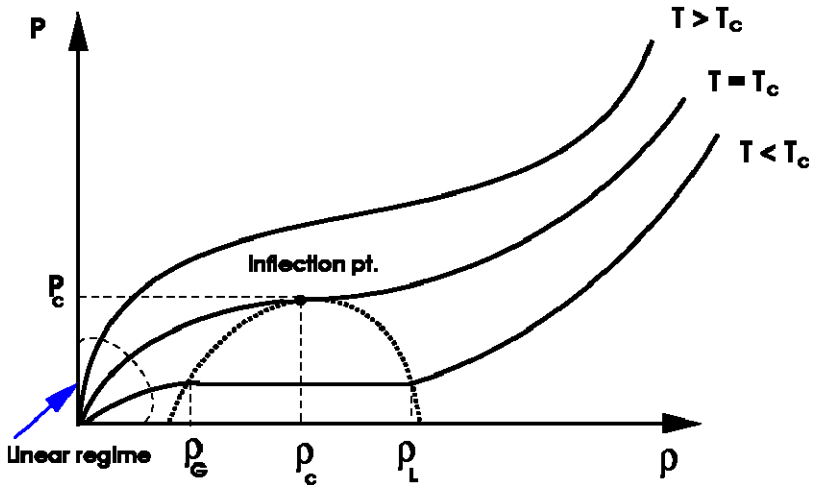

Figure 1.2: A set of isotherms of the equation of state for a typical substance. ρ_G, ρ_c and ρ_L correspond to vapor density, density of the substance at critical point and liquid density respectively.

The equation of state of a system can be expressed as a function of density and temperature in the form

$$P = g(\rho, T)$$

A set of isotherms of the equation of state for a typical substance might appear as shown in figure 1.2.

According to figure 1.2, the dashed curve corresponds to the gas-liquid coexistence curve and the projections explain the qualitative features of the critical point. Below the critical isotherm, the gas-liquid coexistence curve describes how large a discontinuous change in the density occurs during first-order gas-liquid phase transition which means at low temperatures there is a rather large difference between the liquid and gas densities, ρ_L and ρ_G However, at the inflection point, which corresponds to the critical point, as the critical temperature is approached these densities difference tend to zero. The existence of a quantity which is non-zero below the critical temperature and zero above it will be seen to be a common feature associated with the critical points of a wide variety of physical systems. It can be said that ρ_L - ρ_G, is the order parameter for the liquid-gas critical point where the order parameter is defined a thermodynamic function that is different in each phase.

As noted above, the divergences in thermodynamic derivative quantities occur in the same way for systems belonging to the same universality class. These divergences behave as power laws, and hence can be described by the exponents in the power laws. These exponents are known as the critical exponents.

Critical exponents describe the behavior of physical quantities near continuous phase transitions. It is believed, though not proven, that they are universal, i.e. they do not depend on the details of the physical system, but only on

- the dimension of the system,
- the range of the interaction,
- the spin dimension.

These properties of critical exponents are supported by experimental data.

The general definition of a critical-point exponent to describe the behavior near the critical point of a general function f(ε), where

$$\epsilon \equiv \frac{T - T_c}{T_c} = \frac{T}{T_c} - 1$$

serves as a dimensionless variable to measure the difference in temperature from the critical temperature. This function is assumed positive and continuous for sufficiently small, positive values of ε, and that the limit

$$\lambda \equiv \lim_{\varepsilon \to 0} \frac{\ln f(\varepsilon)}{\ln \varepsilon}$$

exists. This limit, λ, is called the critical-point exponent to be associated with the function f(ε). The importance of critical point exponents is that they are measureable while the complete function may not be and there exist a large number of relations among the exponents that arise from fundamental thermodynamic and statistical mechanical considerations and thus transcend any particular system.

1.3 Raman scattering

The scattering of light may be thought of as the redirection of light that takes place when an electromagnetic (EM) wave (i.e. an incident light ray) encounters an obstacle or nonhomogeneity, in our case the scattering material (solid, liquid or gas). As the EM wave interacts with the matter, the electron orbits within the constituent molecules are perturbed periodically with the same frequency (ν_o) as the electric field of the incident wave. The oscillation or perturbation of the electron cloud results in a periodic separation of charge within the molecules, which is called an induced dipole moment. The oscillating induced dipole moment is manifested as a source of EM radiation, thereby resulting in scattered light. The majority of light scattered is emitted at the identical frequency (ν_o) of the incident light, a process referred to as elastic scattering. However, as explained below, additional light is scattered at different frequencies, a process referred to as inelastic scattering. Raman scattering is one such example of inelastic scattering. In summary, the above comments describe the process of light scattering as a complex interaction between the incident EM wave and the material's molecular/atomic structure.

The Raman phenomenon is an inelastic type of light scattering resulting in discrete changes in photon energy due to excitation of molecular vibrations. The Raman spectrum represents a unique vibrational signature of a scattering molecule and can be used for its identification, structural characterization and concentration determination. These features make Raman spectroscopy an excellent analytical tool. When it was discovered in the late 1920s, Raman scattering was characterized as a very inefficient process. Until very recently, low sensitivity, high fluorescence background, and the need for large complex spectrometers and lasers severely hampered applications of Raman spectroscopy in general, and more specifically, its utility in analyzing chemical and biological samples. A dramatic advancement in laser technology and the development of new efficient light detecting arrays have revolutionized Raman spectroscopy during the last decade. It is considered now to be the "process control star" of this century due to unusual, if not unique, compositional information provided by Raman measurements.

Raman scattering has also proven to be a valuable tool in the study of structural phase transitions. In most experiments these transitions are induced by changes in one of the thermodynamic variables temperature or pressure. The effects of increased temperature are usually opposite those of increased pressure, since the former tends to increase the inter-atomic spacings, via thermal expansion, whereas the latter decreases inter-atomic spacings. Normally, the phonon frequencies increase slowly when the lattice contracts, and the relative changes in frequency are small, i.e. on the order of the relative changes in the lattice constants. Deviations from this "normal" behavior often signal a phase transition.

Second order transitions are generally reversible, whereas first-order transitions are not. The most interesting cases for Raman studies are those second order transitions in which a Raman-active mode has the correct symmetry to induce the transition from one phase to the other.

1.4 Purpose

The mechanism of phase transition in nitrogen and benzene has been studied using Raman spectroscopy. The purpose of this thesis is to calculate the Raman frequencies of some lattice and internal modes using volume data from literature.

In chapter 2, the Raman frequencies of the lattice modes using the experimental molar volume through the mode Grüneisen parameter in the β phase of solid nitrogen and in chapter 3, the Raman frequencies of different phases of solid and liquid benzene have been calculated. Conclusions are given in chapter 4.

CHAPTER 2

RAMAN STUDY OF SOLID NITROGEN IN THE β PHASE AND CLOSE TO THE MELTING LINE

2.1 Introduction

Molecular nitrogen (N_2) has many solid phases under various temperatures and pressures, as shown in V-T [6] and T-P [7-9] phase diagrams. At low pressures below 3 kbar, it has a cubic α phase with four molecules per unit cell [10] as an ordered phase. As the temperature increases, there occurs a disordered hexagonal β phase which is adjacent to the melting curve [11]. Beyond 3.5 kbar, the solid N_2 has an ordered tetragonal γ phase with two molecules per unit cell [12, 13]. At room temperature above 4.5 GPa, a cubic disordered δ phase occurs [14]. This phase is transformed into the partially-ordered δ_{loc} - N_2 phase and to a completely-ordered Є-N_2 phase with decreasing temperature (or increasing pressure)[9]. At higher pressures above 100 GPa, ξ-N_2 phase occurs, below this pressure at around 65 GPa (above 750 K) the i-N_2 and Θ-N_2 (~ 850 K at 69 GPa) phases have also been obtained by Raman spectroscopy [9]. At around 200 GPa (300 K) the η phase has been detected by using high pressure Raman spectroscopy [15].

Various experimental techniques have been used to explain the mechanism of transitions among the phases in solid nitrogen. Measurements of the thermal expansivity [16, 17], the specific heat [18] have been made. Spectroscopic techniques such as X-ray [14, 19], infrared [9] and Raman [6, 7, 9, 15, 20-25] have been used widely to investigate the phase transitions in solid nitrogen.

Some theoretical studies on the phase transitions in solid nitrogen have also been reported in literature [26-32]. We have calculated the temperature dependence of the Raman frequencies from the anharmonic self energy for solid nitrogen in our recent studies [33, 34].

In this study, we calculate the Raman frequencies of the lattice modes using the experimental molar volume [6] through the mode Grüneisen parameter in the β phase of solid nitrogen. The lattice modes studied here are the low – and high – frequency Raman lines identified with translational and librational modes, respectively [6]. By using the experimental values [6] of the mode Grüneisen parameter which are assumed to remain constant throughout the β phase, the Raman frequencies of those lattice modes are predicted.

Below, in section 2.2 we give our calculations and results. In section 2.3, our results are discussed. Conclusions are given in chapter 4.

2.2 Calculations and Results

In molecular crystals, the mode Grüneisen parameter can be defined as

$$\gamma_j = -\frac{d \ln \nu_j}{d \ln V} \tag{2.1}$$

where ν_j is the frequency of the j^{th} mode and V is the crystal volume. Since the frequency and the volume can depend on the temperature and pressure, the isobaric (γ_p) and isothermal (γ_T) mode Grüneisen parameters can also be defined as

$$\gamma_p = -\frac{(\partial \ln \nu / \partial T)_p}{(\partial \ln V / \partial T)_p} \tag{2.2}$$

and

$$\gamma_T = -\frac{(\partial \ln \nu / \partial P)_T}{(\partial \ln V / \partial P)_T} \tag{2.3}$$

respectively.

By considering the temperature dependence of both the frequency and the crystal volume, the mode frequency can be expressed as a function of temperature using Eq. (2.2) as follows:

$$\nu_P(T) = A(T,P) + \nu_1 exp[-\gamma_P \ln\left(\frac{V_P(T)}{V_1}\right)] \quad (2.4)$$

where we assume the temperature and pressure dependence of the additional term as

$$A(T,P) = a + bT + cP + dP^2 \quad (2.5)$$

with the constant coefficients a, b, c and d.

In Eq. (2.4) ν_1 and V_1 represent the frequency and volume at a constant temperature and pressure.

In this study we predicted the temperature dependence of the Raman frequency for the lattice modes of ~36 cm^{-1} and 68 cm^{-1} (55 K) by using the experimental volume data [6] in the β phase of solid nitrogen according to Eq. (2.4). For this prediction of the Raman frequencies of the lattice modes studied, on the basis of the observed data for the Raman frequencies and the crystal volume [6] we assumed the pressure dependence of the volume and the Raman frequency as

$$V = a_0 + a_1 P + a_2 P^2 \quad (2.6)$$

and

$$\nu = b_0 + b_1 P + b_2 P^2 \quad (2.7)$$

respectively, with the constants a_0, a_1, a_2, b_0, b_1 and b_2. Table 2.1 gives the values of the volume and Raman frequencies of the lattice modes with the uncertainties which were measured at various pressures at a constant temperature of 55 K in the β phase of solid nitrogen [6]. We first analyzed this observed data from the literature [6] according to Eqs. (2.6) and (2.7). Coefficients of the volume (Eq. 2.6)

and of the Raman frequency for the lattice modes (Eq. 2.7), which we determined from our analysis, are given in Tables 2.2 and 2.3, respectively.

Table 2.1 Experimental values of the molar volume V and the Raman frequencies ν of the low- and high- frequency modes with uncertainties [6] at various pressures at 55 K for the β phase of solid nitrogen.

P(kbar)	V(cm^3/mole)	ν(cm^{-1})	ν(cm^{-1})
2.85	26.87±0.08	25±3	50±3
4.28	25.90±0.09	28±3	54±3
6.00	25.05±0.09	31±3	58±3
9.75	23.59±0.10	36±3	68±3

Table 2.2 Values of the coefficients a_0, a_1 and a_2 which were obtained from the observed data for the molar volume [6] at various pressures (T=55 K) according to Eq. (2.6) in the β phase of solid nitrogen.

V(cm^3/mole)	a_0(cm^3/mole)	a_1(cm^3/mole.kbar)	a_2(cm^3/mole.$kbar^2$)
	28.9837	-0.819	0.027

Table 2.3 Values of the coefficients b_0, b_1 and b_2 which were obtained from the observed Raman frequencies of the low-frequency (36 cm^{-1}) and high frequency (68 cm^{-1}) modes at various pressures (T=55 K) according to Eq. (2.7) in the β phase of solid nitrogen. Values of the mode Grüneisen parameter γ_P with the uncertainties [6] for both lattice modes in the β phase of solid nitrogen are given here. Values of the coefficients c_0 and c_1 (Eq. 2.8) are also given here.

ν(cm^{-1})	b_0(cm^{-1})	b_1(cm^{-1}/kbar)	b_2(cm^{-1}/$kbar^2$)	γ_P	c_0(cm^{-1})	$-c_1$(cm^{-1})
36	18.16	2.637	-0.083	2.8 ± 0.5	40.76	0.085
68	43.08	2.377	0.018	2.4 ± 0.5	68.67	0.017

We then determined the coefficients a, b, c and d in Eq. (2.5) by using the observed data for the molar volume V(P) and ν(P) at 55 K [6] as the initial data for the β phase of solid nitrogen, as given in Table 2.1. For this determination, we also used as the initial data the values of V_1, ν_1 and γ_p for both lattice modes in Eq. (2.4). The values of V_1 and ν_1 were determined at P=0 (T= 55 K) according to Eqs. (2.6) and (2.7), respectively, which are denoted as a_0 for V_1 (Table 2.2) and b_0 for ν_1 (Table 2.3). We also used in Eq. (2.4) the observed values [6] of the mode Grüneisen parameter γ_T for both lattice modes in the β phase (T=55 K), as given in Table 2.3. By solving the coefficients a, b, c and d from four equations, the Raman frequencies were finally predicted as a function of temperature for the low-frequency and high-frequency modes in the β phase of solid nitrogen. The coefficients a, b, c and d which we determined for both lattice modes are given in Table 2.5. In order to solve the coefficients a, b, c and d using Eq. (2.4), we also used the observed volume value of 23.75 cm^3/mole [6] at the melting temperature (T=189 K, P=9.75 kbar) between the β phase and the fluid. The corresponding Raman frequencies of the low-frequency mode and of the high-frequency mode were obtained by extrapolating the observed Raman data [6], as given in Table 2.4. According to a linear fit,

$$\nu = c_0 + c_1 T \tag{2.8}$$

c_0 and c_1 values were determined for both the lattice modes, which we tabulate in Table 2.3. Since we used the observed data for the volume (Table 2.6) at the melting point (P=9.75 kbar, T=189 K) to determine the coefficients a, b, c and d, within the pressure range studied for the β phase, the Raman frequencies of the two lattice modes were predicted for the melting pressures (temperatures) according to Eq. (2.4). For this prediction, the observed volume data [6] at the melting points, as given in Table 2.6, were used. The predicted Raman frequencies of the low-frequency and high-frequency modes are also given in Table 2.6.

Table 2.4 Observed values of the Raman frequencies for the low- and high-frequency modes with the uncertainties [6] at various temperatures (P=9.75 kbar), which were used to determine the coefficients a, b, c and d (Eq. 2.5).

T(K)	$\nu(cm^{-1})$	$\nu(cm^{-1})$
55	36±3	68±3
80	34±4	67±4
102	32±4	67±4
135	30±5	66±5
170	26±5	66±5

Table 2.5 Values of the coefficients a, b, c and d (Eq. 2.5) which were obtained for the Raman modes indicated in the β phase of solid nitrogen.

$\nu(cm^{-1})$	a (cm^{-1})	$-b(cm^{-1}/K)$	$c(cm^{-1}/kbar)$	$d(cm^{-1}/kbar^2)$
ν_{low} mode	5.249	0.084	0.819	-0.052
ν_{high} mode	2.238	0.019	-1.245	0.088

Table 2.6 Observed data for the molar volume [6] at the melting pressures and temperatures along the melting curve of the β phase – fluid in nitrogen. Calculated Raman frequencies of the low- and high- frequency modes (Eq. 2.4) are also given here.

P (kbar)	T (K)	V $(cm^3/mole)$	$\nu(cm^{-1})$	$\nu(cm^{-1})$
2.85	112	26.94	20.4	48.6
4.28	131	26.00	21.4	51.9
6.00	151	25.15	22.7	55.6
9.75	189	23.75	24.2	64.3

We also predicted here the temperature dependence of the crystal volume at P=9.75 kbar in the β phase of solid nitrogen. The molar volume was predicted by using the relation

$$V_P(T) = V_1 exp[-\frac{1}{\gamma_P} ln[\frac{\nu_P - A(T,P)}{\nu_1}] \quad (2.9)$$

which was obtained from Eq. (2.4) with Eq. (2.5). We first predicted the molar volume at 55K (P= 9.75 kbar) by using the observed values of the low-frequency and high-frequency modes (Table 2.1) according to Eq. (2.9), which we obtained the same value of 23.59 cm^3/mole. We then predicted at various temperatures (P=9.75 kbar) the molar volumes in the β phase of solid nitrogen by Eq. (2.9) using the observed Raman frequencies of the high-frequency mode (Table 2.4).

Finally, the calculated values of the molar volume were used to predict the temperature dependence of the Raman frequencies of the low-frequency mode according to Eq. (2.4), as plotted in Fig. 2.1. Also, by using the calculated values of the molar volume in Eq. (2.4), the temperature dependence of the Raman frequencies of the high-frequency mode were predicted, as plotted in Fig. 2.2. In Figs. 2.1 and 2.2, the observed Raman frequencies of the two lattice modes are also plotted.

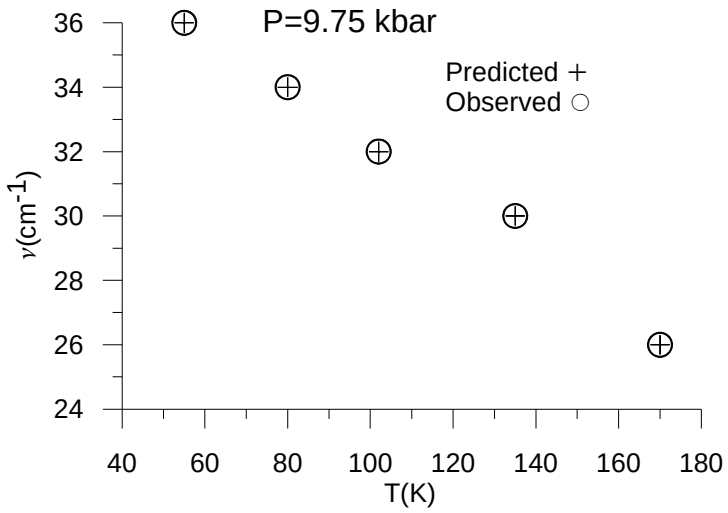

Figure 2.1 Raman frequencies calculated as a function of temperature for the low-frequency mode according to Eq. (2.4) using the molar volume data [6] at P=9.75 kbar in the β phase of solid nitrogen. Observed Raman frequencies [6] are also shown here.

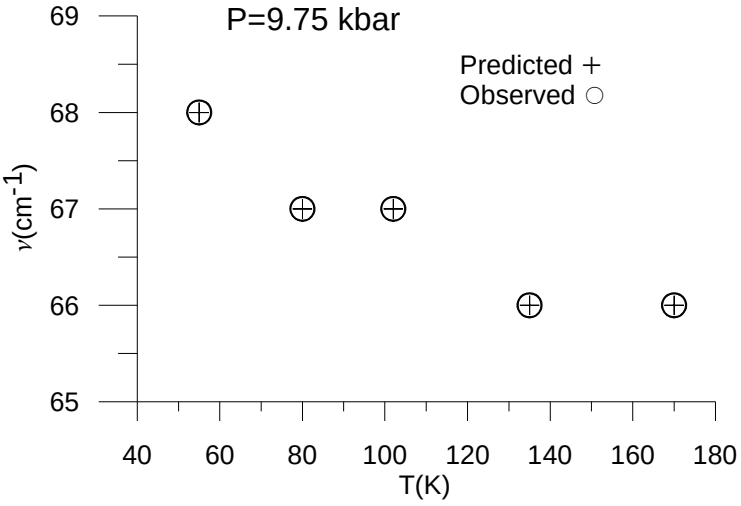

Figure 2.2 Raman frequencies calculated as a function of temperature for the high-frequency mode according to Eq. (2.4) using the molar volume data [6] at P=9.75 kbar in the β phase of solid nitrogen. Observed Raman frequencies [6] are also shown here.

Similarly, the Raman frequencies of the low- and high- frequency modes were calculated (Eq. 2.4) by using the volume data (Table 2.6) along the melting curve (β-phase – fluid) of solid nitrogen. Figs. 2.3 and 2.4 give our calculated Raman frequencies along the melting curve (β - fluid) as a function of pressure for the low- and high- frequency modes, respectively. A similar calculation was conducted for both the lattice modes and the Raman frequencies were calculated as a function of pressure at a constant temperature of 55 K, as plotted in Figs. 2.5 and 2.6 with the observed Raman data. Eq. (2.4) was used for this calculation, as we also calculated the Raman frequencies at various temperatures for a constant pressure of P=9.75 kbar (Figs. 2.1 and 2.2).

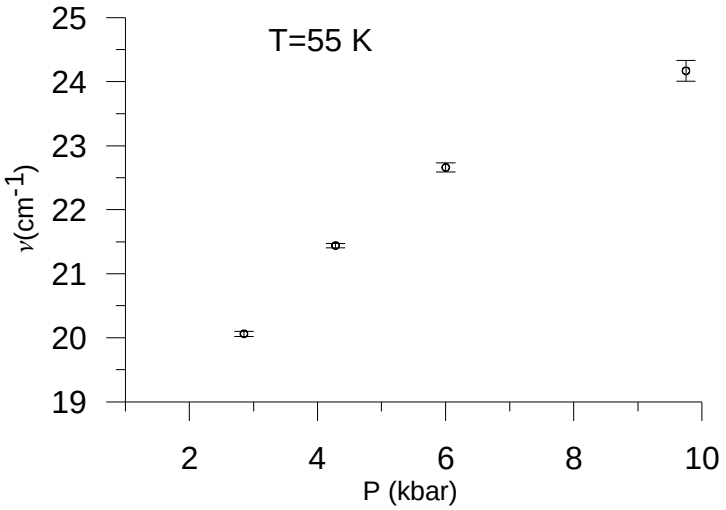

Figure 2.3 Raman frequencies calculated as a function of pressure at the melting points along the melting curve (β - fluid) for the low-frequency mode according to Eq. (2.4) in nitrogen.

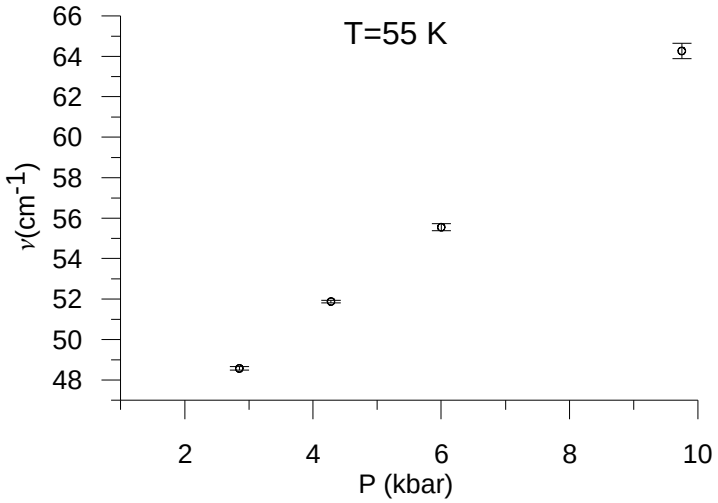

Figure 2.4 Raman frequencies calculated as a function of pressure at the melting points along the melting curve (β - fluid) for the high-frequency mode according to Eq. (2.4) in nitrogen.

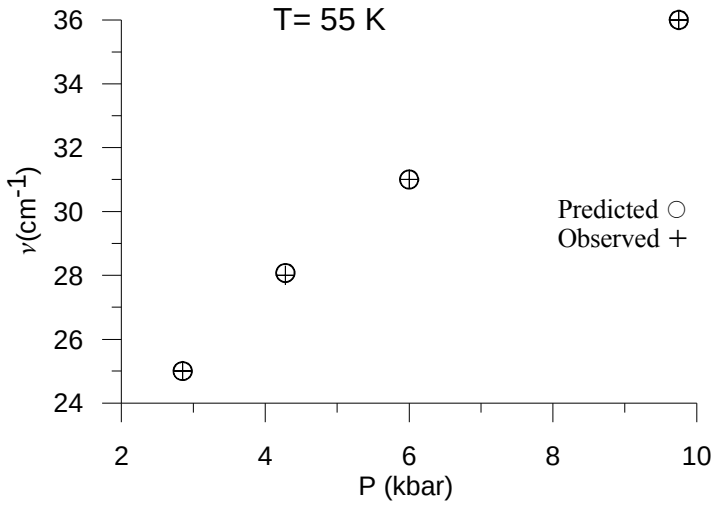

Figure 2.5 Calculated Raman frequencies of the low-frequency mode as a function of pressure (T=55 K) in the β phase of solid nitrogen according to Eq. (2.4). Experimental values [6] are also shown here.

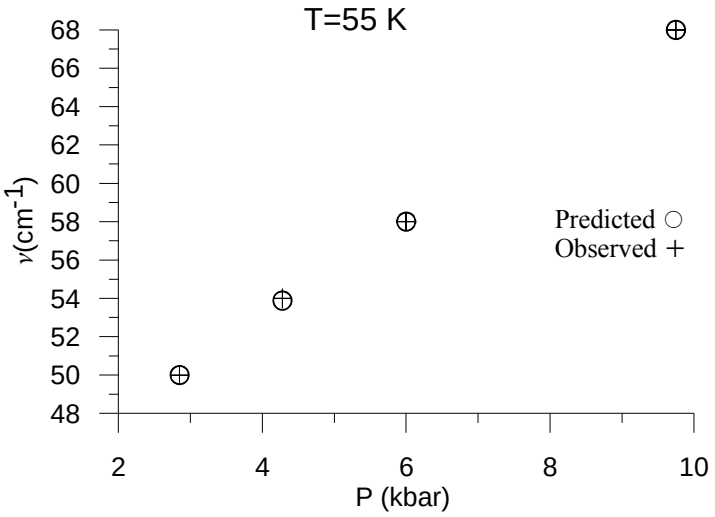

Figure 2.6 Calculated Raman frequencies of the high-frequency mode as a function of pressure (T=55K) in the β phase of solid nitrogen according to Eq. (2.4). Experimental values [6] are also shown here.

2.3 Discussion

The Raman frequencies of the two lattice modes were calculated here as a function of temperature at P=9.75 kbar (Figs. 2.1 and 2.2) and as a function of pressure at T=55 K (Figs. 2.5 and 2.6) in the β phase of solid nitrogen. The pressure (or temperature) dependence of the Raman frequencies for these two modes was also calculated at the melting points along the melting curve (β-fluid), as shown in Figs. 2.3 and 2.4. The experimental data for the molar volume was used through the mode Grüneisen parameter γ_P for this calculation of the Raman frequencies of the lattice modes considered. As shown in Figs. 2.1 and 2.2, the Raman frequencies of the low- frequency and high – frequency modes decrease with increasing temperature in the β phase of solid nitrogen, as expected. Also, the Raman frequencies of the lattice modes studied here increase with increasing pressure at the melting points (Figs. 2.3 and 2.4) and at 55 K in the β phase of this molecular solid (Figs. 2.5 and 2.6). As shown in these figures (Figs. 2.1-2.6), our calculated Raman frequencies of both the low- and high- frequency modes are in agreement with the observed Raman data [6]. Since the uncertainties in the

experimental measurements of the Raman frequencies for the lattice modes are considerably large (Tables 2.1 and 2.4), our calculated Raman frequencies should be considered within those uncertainties. Also, there is an uncertainty of ±0.5 for the Grüneisen parameter γ_P for both lattice modes (Table 2.3), which can change our calculated Raman frequencies through the coefficient b_0 (Table 2.3) and some variations in the coefficients a, b, c and d (Table 2.5).

This increase in the Raman frequency as the temperature decreases (Figs. 2.1 and 2.2) and also as the pressure increases (Figs. 2.3-2.6), indicates that the N_2 molecules become more ordered in the β phase. This is due to the fact that the vibrational frequency depends on the orientation of the molecules [35] in the absence of the vibrational coupling in the disordered β phase [36], where the N_2 molecules rotate in two dimensions which describe disks [37, 38]. X-ray diffraction studies have indicated that there is a high degree orientational disorder in the β phase, as also pointed out previously [6].

The pressure dependence of the Raman frequencies has also been observed experimentally in various phases of solid N_2. The Raman frequencies of the lattice modes increase with decreasing molar volumes [6], as we also studied here in the β phase, and the ν_1 and ν_2 vibrons shift to higher frequencies with increasing pressure in the pressure range of 8 to 54 GPa at room temperature. On the contrary, the Raman frequency decreases as the pressure increases in the γ phase for the lattice modes (γ-N_2 at T = 15 K , P=0.49 GPa for the 55 cm^{-1} and 97 cm^{-1} modes) [7].

Regarding the temperature dependence of the Raman frequencies of the lattice modes, as studied here, the Raman frequencies of the low- and high-frequency modes decrease with increasing temperature in the β phase, which we have also obtained in our previous study [33]. In the γ phase of solid nitrogen, the Raman frequencies of the lattice modes (58 cm^{-1} and 100 cm^{-1}) also decrease, whereas the internal mode (2330 cm^{-1}) increases unexpectedly with increasing temperature, as we have reported previously [33] on the basis of the experimental data [6]. However, along the melting curve between the solid β phase and the fluid, the Raman frequencies of the low- and high- frequency modes increase as the

melting temperature (or melting pressure) increases (Table 2.6), as shown in Figs. 2.3 and 2.4 in this study. Molecular dynamic simulations can be performed to explain the mechanism of transition from the liquid to the solid phase, as studied previously [28].

CHAPTER 3

RAMAN STUDY OF BENZENE AS A FUNCTION OF PRESSURE AT CONSTANT TEMPERATURES NEAR THE MELTING POINT

3.1 Introduction

Benzene (C_6H_6) is the most studied aromatic compound. At atmospheric pressure below the melting point (T_m=278.6 K), it crystallizes into the solid phase I [39]. In this phase benzene has four molecules per unit cell. At 1.2 GPa as the temperature increases up to 373 K, phase I transforms into the solid phase II.[40]. Experimental studies have revealed that the transition from phase II to phase III occurs at 3.5 GPa at room temperature and that a fourth phase occurs [41] as shown in the T-P phase diagram [42, 43], which we give here in Fig. 3.1. Transition from the solid to the liquid phase has also been studied and the pretransition effects prior to the melting in benzene have been investigated [44, 45]. It has many solid phases, liquid phase and also polymer phases (Fig. 3.1). At room temperature (25^{o}C) the solid benzene melts into the liquid phase at about 70 MPa [44].

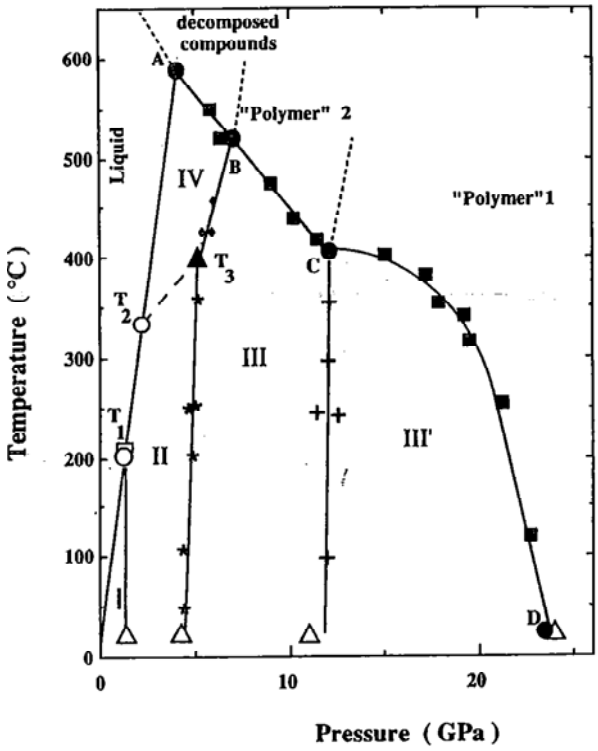

Figure 3.1 Phase diagram of benzene. The melting curve is from Ref. [55]; the triple points T1 and T2 are from Ref. [53] (o) and [40]. The phase transitions of solid benzene (Δ) at ambient temperature are from Ref. [55]. The chemical decomposition point A is from Ref. [55]. From this work: (1) benzene II-benzene III transition line (*); (2) benzene III-benzene III′ transition line (+); (3) benzene IV-benzene III transition line(♦); (4) chemical transformation line (■) defined by A, B, C, D points. The phase transition line between II and IV (dashed line) and the limits between the domains of polymer1, polymer 2, and decomposed compounds domain are speculative.

Phase transitions in benzene have been investigated extensively using various experimental techniques and also some theoretical models. As a plastic reorientational crystal, many years ago Bridgman [46] performed volumetric measurements for the phase I – phase II transformation in solid benzene. Near the melting point, it has been studied spectroscopically [44, 47, 48] and thermodynamically [44, 45, 49]. The Raman study focusing on the phase II of benzene has been reported [43]. Molar volume of benzene has been calculated close to the melting point as functions of temperature [50] and pressure [51] in recent studies. Using the Raman date [43], vibrational frequencies of the lattice

modes have been calculated at various pressures in phase II of solid benzene very recently [52].

The complex vibrations of a molecule are the superposition of relatively simple vibrations called the normal modes of vibration. Each normal mode of vibration has a fixed frequency. Selection rules tell us if a transition is allowed or forbidden. An allowed transition has a high probability of occurring and will result in a strong band. If a normal mode has an allowed Raman transition, it is said to be Raman active. In the lattice regions, factor group analysis predicts 12 Raman active librational modes $3A_g + 3B_{1g} + 3B_{2g} + 3B_{3g}$ in benzene I and 6 Raman active librational modes $3 A_g + 3B_g$ in Benzene III, with the proposed structures [41].

In this study, we calculate the Raman frequencies for the lattice modes of A_g, A_gB_{2g} and $B_{1g}B_{3g}$ in benzene as a function of pressure for constant temperatures of 252, 275 and 296 K by using the volume data [44]. This calculation of the Raman frequencies is performed by means of the mode Grüneisen parameter. Our calculated Raman frequencies are compared with the observed Raman frequencies [48] of the modes studied here.

3.2 Calculations and Results

The Raman frequencies $\nu_T(P)$ at constant temperature using the volume $V_T(P)$ as a function of pressure can be expressed as

$$\upsilon_T(P) = \upsilon_1 \exp[-\gamma_T ln \frac{V_T(P)}{V_1}] \tag{3.1}$$

In Eq (3.1) V_1 is the crystal volume and ν_1 is the Raman frequency at constant temperature and pressure.

In this study we predicted the Raman frequency for the lattice modes of A_g, A_gB_{2g}, and $B_{1g}B_{3g}$ using the experimental volume data [44] of solid and liquid benzene according to Eq. (3.1). For this prediction of the Raman frequencies of the lattice modes studied on the basis of the observed data for the Raman frequencies

[48] and the crystal volume [44], we assumed the pressure dependence of the volume and the Raman frequency as

$$V = a_0 + a_1 P + a_2 P^2 \tag{3.2}$$

and

$$\nu = b_0 + b_1 P + b_2 P^2 \tag{3.3}$$

respectively, with the constants a_0, a_1, a_2, b_0, b_1 and b_2.

Table 3.1 gives the values of the coefficients a_0, a_1 and a_2 according to Eq. (3.2) which was fitted to the experimental data for the molar volumes of solid benzene [44]. We also analyzed the observed data (given in Table 3.2) from the Ref. [48] according to Eq. (3.3) and the coefficients b_0, b_1 and b_2 for the Raman frequency of the lattice modes A_g, A_gB_{2g}, and $B_{1g}B_{3g}$ were determined. They are tabulated in Table 3.3.

Table 3.1 Values of the coefficients according to Eq. (3.2) which was fitted to the experimental data for the molar volumes of solid benzene lower than 73×10^{-6} m^3. Values in parentheses take into account the maximum possible error [44].

T(K)	a_0 ($m^3.mol^{-1} \times 10^{-6}$)	$-a_1$ ($m^3.mol^{-1}MPa^{-1} \times 10^{-6}$)	a_2 ($m^3.mol^{-1}MPa^{-2} \times 10^{-6}$)	Pressure Range (MPa)
253	73.739 (73.540)	1.368×10^{-2} (1.453×10^{-2})	1.612×10^{-6} (1.771×10^{-6})	50 – 400
298	75.482 (75.239)	1.642×10^{-2} (1.732×10^{-2})	5.355×10^{-6} (5.552×10^{-6})	160 – 490
273	74.351 (74.239)	1.410×10^{-2} (1.497×10^{-2})	2.467×10^{-6} (2.632×10^{-6})	100 – 430
301.5	75.522 (75.537)	1.490×10^{-2} (1.582×10^{-2})	2.373×10^{-6} (2.552×10^{-6})	180 – 420
313	76.953 (77.022)	2.136×10^{-2} (2.231×10^{-2})	11.543×10^{-6} (11.810×10^{-6})	200 – 450
324	77.331 (77.452)	2.091×10^{-2} (2.187×10^{-2})	10.114×10^{-6} (10.381×10^{-6})	230 – 480

Table 3.2 Raman frequencies of the A_g, A_gB_{2g}, and $B_{1g}B_{3g}$ modes along some of the "Isospectrum" lines in solid benzene [48].

	252 K		275 K		296K	
A_g	P(kbar)	$\nu(cm^{-1})$	P(kbar)	$\nu(cm^{-1})$	P(kbar)	$\nu(cm^{-1})$
	5.370	58	5.45	59	6.525	57
	4.750	56.8	4.87	56.5	5.96	56
	3.510	53.6	3.84	53.5	4.71	53.7
	1.820	46.5	2.1	46	2.77	46
	252 K		275 K		296K	
A_gB_{2g}	P(kbar)	$\nu(cm^{-1})$	P(kbar)	$\nu(cm^{-1})$	P(kbar)	$\nu(cm^{-1})$
	5.370	84	5.45	84.5	6.525	83
	4.750	82.2	4.87	82.8	5.96	82
	3.510	79	3.84	79.5	4.71	79.5
	1.820	74	2.1	72.74	2.77	74
	252 K		275 K		296K	
$B_{1g}B_{3g}$	P(kbar)	$\nu(cm^{-1})$	P(kbar)	$\nu(cm^{-1})$	P(kbar)	$\nu(cm^{-1})$
	5.370	139	5.45	139	6.525	139
	4.750	136	4.87	136	5.96	136
	3.510	130	3.84	130	4.71	130
	1.820	120	2.1	120	2.77	120

Table 3.3 Values of the coefficients b_0, b_1 and b_2 according to Eq. (3.3) which was fitted in this study to the experimental data [48] for the observed frequencies of the Raman modes indicated at 252, 275 and 296 K in solid benzene. Values of the Grüneisen parameter γ_T, obtained from Eq. (3.4) for the Raman modes are also given here.

	Raman Modes	$b_0(cm^{-1})$	$b_1(cm^{-1}/bar)$	$b_2(cm^{-1}/bar^2)$	$\gamma_T(P = 1.82kbar)$
T=252K	A_g	35.55	6.96	-0.517	5.9
	A_gB_{2g}	68.13	3.36	-0.076	2.3
	$B_{1g}B_{3g}$	107.29	7.54	-0.304	2.9
	Raman Modes	$b_0(cm^{-1})$	$b_1(cm^{-1}/bar)$	$b_2(cm^{-1}/bar^2)$	$\gamma_T(P = 2.1kbar)$
T=275K	A_g	34.80	5.90	-0.267	5.7
	A_gB_{2g}	62.71	5.27	-0.233	3.2
	$B_{1g}B_{3g}$	107.55	6.03	-0.047	2.7
	Raman Modes	$b_0(cm^{-1})$	$b_1(cm^{-1}/bar)$	$b_2(cm^{-1}/bar^2)$	$\gamma_T(P = 2.77kbar)$
T=296K	A_g	27.53	8.25	-0.573	5.9
	A_gB_{2g}	63.0	4.64	-0.241	2.4
	$B_{1g}B_{3g}$	105.04	5.55	-0.052	2.3

The isothermal mode Grüneisen parameter for each Raman mode was calculated according to

$$\gamma_T = -\frac{\partial ln\nu}{\partial lnV} = -\frac{V}{\nu}(\frac{\partial \nu}{\partial P})_T/(\frac{\partial V}{\partial P})_T \quad (3.4)$$

By using Eq. (3. 2) and Eq. (3.3)

$$(\frac{\partial V}{\partial P})_T = a_1(T) + 2a_2(T)P \quad (3.5)$$

and

$$(\frac{\partial \nu}{\partial P})_T = b_1(T) + 2b_2(T)P \quad (3.6)$$

can be obtained respectively.

Substituting Eqs. (3.5) and (3.6) into Eq. (3.4) and using the values from Tables 3.2 and 3.3 first, we calculated the mode Grüneisen parameter for pressures 1.82 kbar, 2.1 kbar and 2.77 kbar at constant temperatures of 252, 275 and 296 K, respectively. They are tabulated in Table 3.3. By using the volume values (Eq. 3.2) and the Grüneisen parameter γ_T for each mode studied here at constant temperatures of 252, 275 and 296 K, the Raman frequencies of the A_g, A_gB_{2g}, and $B_{1g}B_{3g}$ were calculated as a function of pressure through Eq. (3.1).

The predicted Raman frequencies of the A_g, A_gB_{2g}, and $B_{1g}B_{3g}$ modes are given in Table 3.4 and they are plotted in Figs. 3.2 - 3.4 where the observed Raman frequencies of the three lattice modes are shown for comparison [48].

Table 3.4 Calculated Raman frequencies by using mode Grüneisen parameters given in Table 3.3 for the Raman modes A_g, A_gB_{2g}, and $B_{1g}B_{3g}$ according to Eq. (3.1) for T=252, 275 and 296 K respectively in solid benzene.

T=252 K	$\nu_T(cm^{-1})$		
P (kbar)	A_g	A_gB_{2g}	$B_{1g}B_{3g}$
5.370	63.6	85.1	142.8
4.750	59.6	83.0	138.2
3.510	52.1	78.9	129.5
1.820	43.4	73.5	118.3
T=275 K	ν_T (cm^{-1})		
P (kbar)	A_g	A_gB_{2g}	$B_{1g}B_{3g}$
5.450	60.8	86.1	139.6
4.870	57.5	83.4	136.0
3.840	51.9	78.7	129.7
2.100	43.5	71.1	119.3
T=296K	ν_T (cm^{-1})		
P (kbar)	A_g	A_gB_{2g}	$B_{1g}B_{3g}$
6.525	55.1	83.4	138.3
5.960	52.5	81.8	135.7
4.710	46.8	78.1	129.7
2.770	38.3	72.0	119.7

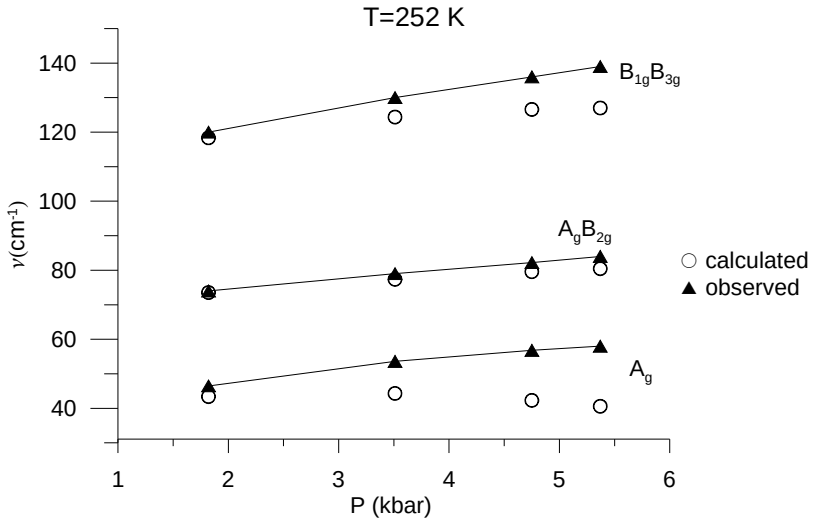

Figure 3.2 Raman frequencies calculated as a function of pressure for the Raman modes A_g, A_gB_{2g}, and $B_{1g}B_{3g}$ according to Eq. (3.1) at T=252 K for solid benzene. The observed Raman frequencies are also shown here [48].

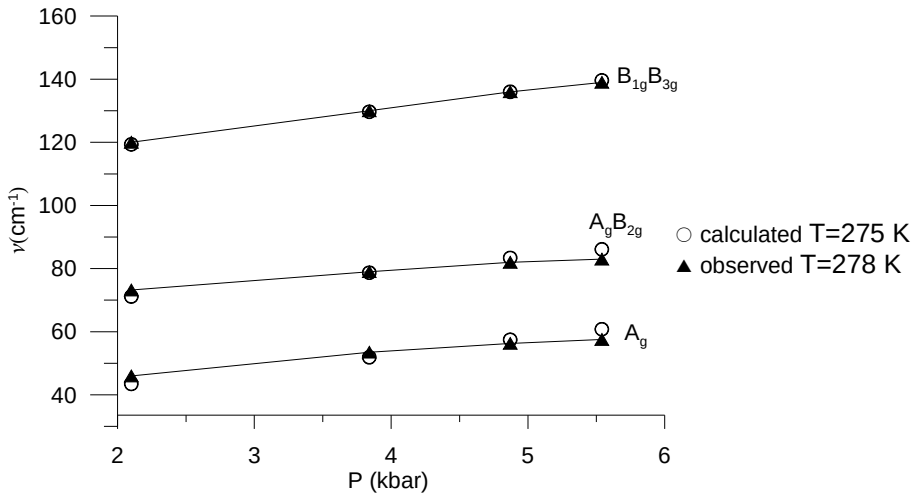

Figure 3.3 Raman frequencies calculated as a function of pressure for the Raman modes A_g, A_gB_{2g}, and $B_{1g}B_{3g}$ according to Eq. (3.1) at T=275 K for solid benzene. The observed Raman frequencies at 278 K are also shown here [48].

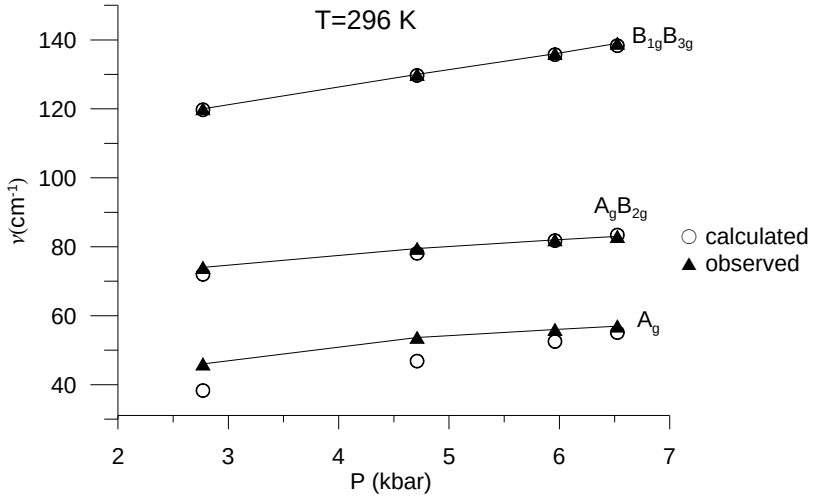

Figure 3.4 Raman frequencies calculated as a function of pressure for the Raman modes A_g, A_gB_{2g}, and $B_{1g}B_{3g}$ according to Eq. (3.1) at T=296 K for solid benzene. The observed Raman frequencies are also shown here [48].

According to our results, the predictions are in good agreement with the observed data except for A_g and $B_{1g}B_{3g}$ modes at 252 K. The calculated Raman frequencies are increasing with pressure as expected in A_gB_{2g} mode at T=252 K and in A_g, A_gB_{2g}, and $B_{1g}B_{3g}$ modes at T=275 and 296 K. However, at A_g and

$B_{1g}B_{3g}$ modes at 252 K, the trend in the change of frequency with pressure reverses at pressure values above 3.5 kbar.

Next, we calculated the mode Grüneisen parameters at four different pressures as given in Table 3.5 for constant temperatures of 252, 275 and 296 K and tabulated in Table 3.3. By using these Grüneisen parameters in Eq (3.1) Raman frequencies of the A_g, A_gB_{2g}, and $B_{1g}B_{3g}$ modes are predicted and tabulated in Table 3.5. Results are plotted in Figs. (3.5-3.7) where the observed Raman frequencies of the three lattice modes are shown for comparison [48].

Table 3.5 Calculated Raman frequencies for the Raman modes A_g, A_gB_{2g}, and $B_{1g}B_{3g}$ according to Eq. (3.1) with mode Grüneisen values at four different pressures for constant temperatures of 252, 275 and 296 K.

T=252 K	**A_g**		**A_gB_{2g}**		**$B_{1g}B_{3g}$**	
P (kbar)	γ_T	ν_T(cm^{-1})	γ_T	ν_T(cm^{-1})	γ_T	ν_T(cm^{-1})
5.370	1.35	40.6	1.7	80.4	1.7	127.0
4.750	2.0	42.3	1.8	79.6	1.9	126.6
3.510	3.4	44.3	2.0	77.4	2.3	124.4
1.820	5.9	43.4	2.3	73.5	2.9	118.3
T=275 K	**A_g**		**A_gB_{2g}**		**$B_{1g}B_{3g}$**	
P (kbar)	γ_T	ν_T(cm^{-1})	γ_T	ν_T(cm^{-1})	γ_T	ν_T(cm^{-1})
5.540	3.0	46.7	1.9	75.6	2.3	135.3
4.870	3.4	46.95	2.1	75.5	2.4	132.7
3.840	4.1	46.4	2.5	74.7	2.5	128.0
2.100	5.7	43.5	3.2	71.1	2.7	119.3
T=296 K	**A_g**		**A_gB_{2g}**		**$B_{1g}B_{3g}$**	
P (kbar)	γ_T	ν_T(cm^{-1})	γ_T	ν_T(cm^{-1})	γ_T	ν_T(cm^{-1})
6.525	1.0	30.9	1.3	73.3	2.5	141.0
5.960	1.7	33.3	1.4	73.9	2.4	137.5
4.710	3.2	36.9	1.8	74.2	2.4	130.1
2.770	5.9	38.3	2.4	72.0	2.3	119.7

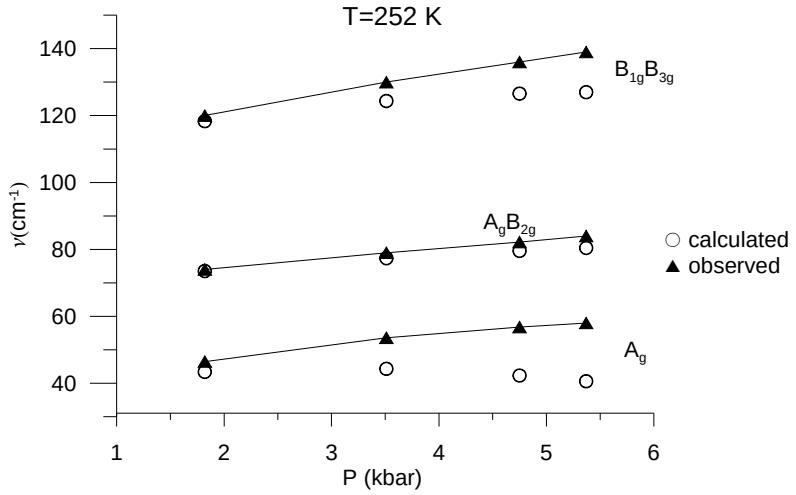

Figure 3.5 Raman frequencies calculated as a function of pressure for the A_g, A_gB_{2g}, and $B_{1g}B_{3g}$ modes according to Eq. (3.1) at 252 K for solid benzene by using the data in Table 3.5. The observed Raman frequencies are also shown here [48].

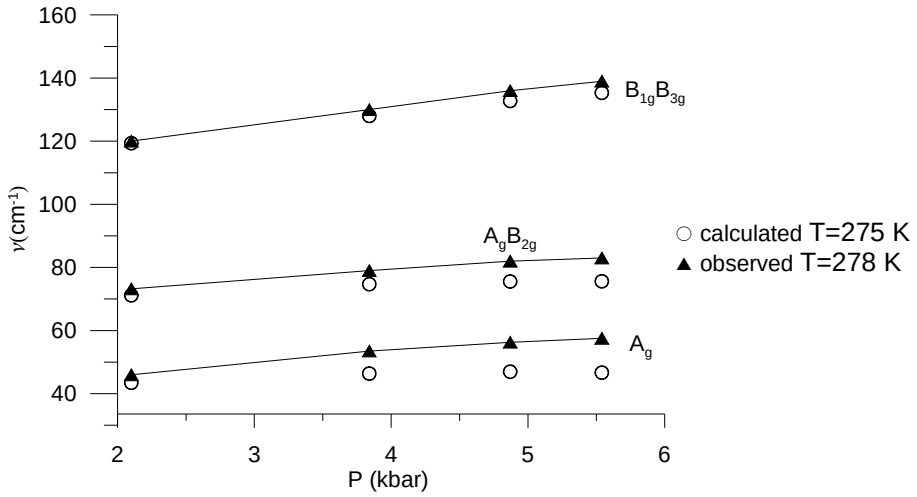

Figure 3.6 Raman frequencies calculated as a function of pressure for the A_g, A_gB_{2g}, and $B_{1g}B_{3g}$ modes according to Eq. (3.1) at 275 K for solid benzene by using the data in Table 3.5. The observed Raman frequencies at 278 K are also shown here [48].

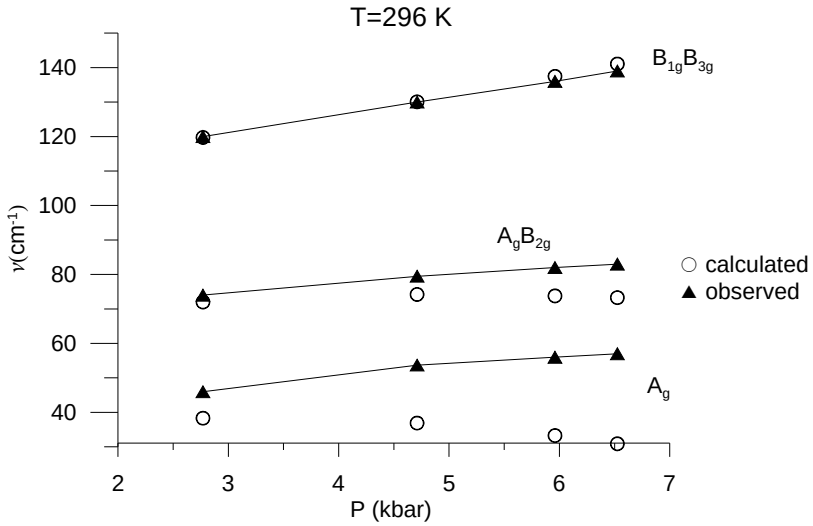

Figure 3.7 Raman frequencies calculated as a function of pressure for the A_g, A_gB_{2g}, and $B_{1g}B_{3g}$ modes according to Eq. (3.1) at T=296 K for solid benzene by using the data in Table 3.5. The observed Raman frequencies are also shown here [48].

So far, we have calculated the Raman frequencies of the A_g, A_gB_{2g}, and $B_{1g}B_{3g}$ modes in the solid phase of benzene as a function of pressure for constant temperatures of 252, 275 and 296 K.

Comparing the results for obtaining the Raman frequencies by calculating the mode Grüneisen parameter as pressure dependent (calculation at a constant pressure) and pressure independent (calculation at four different pressures), the way of predicting the Raman frequencies by calculating pressure independent Grüneisen parameter gives us better fit to the observed data.

In this part of our study, by using Eq. (3.1) and the same values of the mode Grüneisen parameters as in the solid phase, we calculated Raman frequencies for the A_g, A_gB_{2g}, and $B_{1g}B_{3g}$ modes at temperatures 275 and 296 K in the liquid phase of benzene. The results are tabulated in Table 3.6 and Table 3.7 and plotted in Figs 3.8 and 3.9 for temperatures of 275 and 296 K, respectively. Values of a_0, a_1 and a_2 at T=275 K are obtained by fitting the experimental data [44] according to Eq. (3.2) and calculated as

$a_0=77.069 \times 10^{-6}$ ($m^3.mol^{-1}$),

a_1=-7.0023 x10^{-6} (m^3.mol^{-1}.MPa^{-1})

and

a_2=2.7525 x10^{-6} (m^3.mol^{-1}.MPa^{-2})

Table 3.6 Calculated $\nu_T(P)$ values according to Eq. (3.1) for the A_g, A_gB_{2g}, and $B_{1g}B_{3g}$ modes at different pressures for T=275 K in liquid benzene.

T=275 K	$\nu(cm^{-1})$		
P(kbar)	A_g (γ_T= 5.7)	A_gB_{2g} (γ_T=3.2)	$B_{1g}B_{3g}$ (γ_T=2.7)
0.36	40.5	68.4	115.4
0.52	42.7	70.5	118.2
0.90	46.9	74.3	123.5
1,18	48.2	75.5	125.1

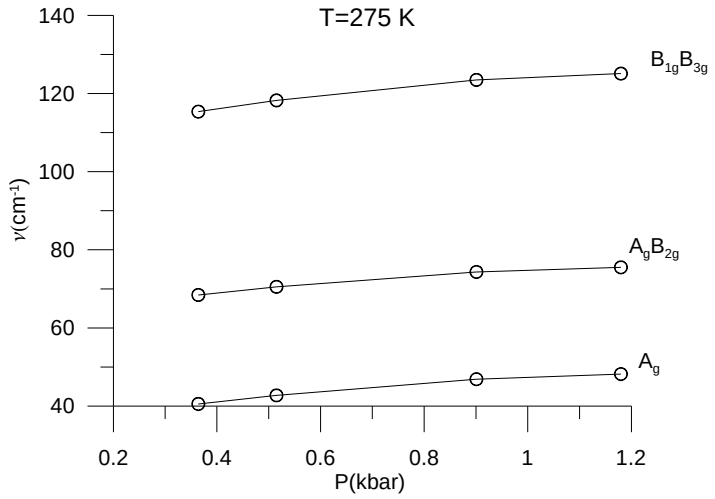

Figure 3.8 Raman frequencies calculated as a function of pressure for the A_g, A_gB_{2g}, and $B_{1g}B_{3g}$ modes according to Eq. (3.1) at T=275 K in liquid benzene by using the data in Table 3.6.

Table 3.7 Calculated ν_T(P) values according to Eq. (3.1). for the A_g, A_gB_{2g}, and $B_{1g}B_{3g}$ modes at different pressures for T=296K in liquid benzene. Values $V_T(p)$ and V_1=$V_m = 83.35\ x10^{-6}\ m^3.mol^{-1}$ were taken from literature [51].

T=296 K		ν (cm^{-1})		
$V_T(P)$x10^{-6} ($m^3.mol^{-1}$)	P(MPa)	A_g (γ_T = 5.9)	A_gB_{2g} (γ_T = 2.4)	$B_{1g}B_{3g}$ (γ_T = 2.3)
89.0	26.30	18.8	53.9	90.2
88.0	31.60	20.0	55.4	92.6
87.3	38.70	21.0	56.5	94.3
86.7	42.10	21.9	57.4	95.9
85.6	44.70	23.6	59.1	98.7
85.0	51.30	24.6	60.1	100.4
84.0	57.90	26.3	61.8	103.2
83.3	63.10	27.6	63.1	105.2
82.6	68.40	29.0	64.4	107.3
80.7	71.00	33.3	68.0	113.2
79.0	71.00	37.7	71.5	119.0
74.3	71.00	54.0	82.7	137.2
73.7	84.60	56.6	84.3	139.8

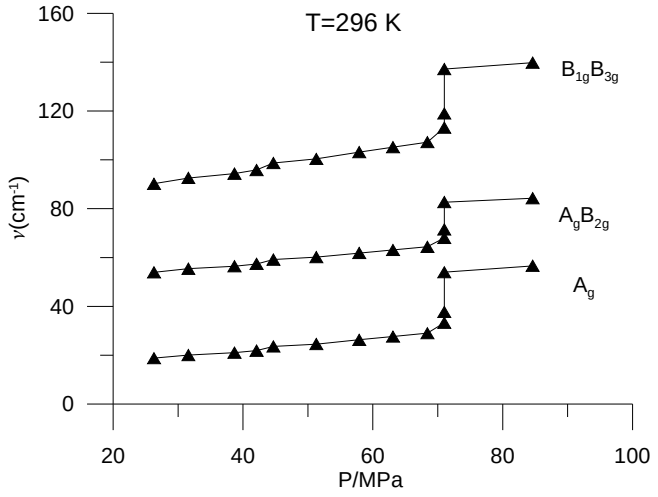

Figure 3.9 Raman frequencies calculated as a function of pressure for the A_g, A_gB_{2g}, and $B_{1g}B_{3g}$ modes according to Eq. (3.1) at T=296 K for liquid benzene by using the data in Table 3.7.

Although there is not an observed data for the Raman frequencies, we predicted the Raman frequencies at constant temperatures of 275 and 296 K by

using our calculated Grüneisen parameters at constant pressures to see the trend in the Raman frequency as a function of pressure in liquid phase. Our results mainly display a similar relationship between the Raman frequencies and the pressure values. Additionaly we obtained an anomalous behavior at above 70 MPa at 296 K.

At this stage, we were also interested in predicting the Raman frequencies of the lattice modes in the solid and liquid phases of benzene by using the values of the mode Grüneisen parameter γ_T extrapolated at zero pressure. For this purpose, we used the pressure dependence of the $\gamma_T(P)$ values according to the relation

$$\gamma_T(P) = c_0 + c_1 P \tag{3.7}$$

Thus, we obtained the coefficients c_0 and c_1 by using data in Table 3.5 and the results are given in Table 3.8. Using these coefficients, values of the extrapolated values of the isothermal mode Grüneisen parameter $\gamma_T(P=0)$ were determined at temperatures of 252, 275 and 296 K in the solid benzene as tabulated in Table 3.8.

Table 3.8 Values of the coefficients c_0 and c_1 (Eq. 3.7) with the mode Grüneisen values at P=0 for T=252, 275 and 296 K.

T=252 K	c_0	$c_1(kbar^{-1})$	$\gamma_T(P=0)$
A_g	8.18	-1.29	8.2
A_gB_{2g}	2.55	-0.16	2.55
$B_{1g}B_{3g}$	3.51	-0.34	3.5
T=275 K	c_0	$c_1(kbar^{-1})$	$\gamma_T(P=0)$
A_g	7.62	-0.82	7.6
A_gB_{2g}	3.43	-0.29	3.4
$B_{1g}B_{3g}$	3.06	-0.16	3.1
T=296K	c_0	$c_1(kbar^{-1})$	$\gamma_T(P=0)$
A_g	9.4	-1.29	9.4
A_gB_{2g}	3.16	-0.29	3.2
$B_{1g}B_{3g}$	2.18	0.04	2.2

The ν_T (P) were then predicted from the volume data according to Eq. (3.1). We used the γ_P value at P=0 for each mode to predict the Raman frequencies for constant temperatures of 252, 275 and 296 K in the solid phase of benzene. The results are given in tables 3.9 - 3.11. The Raman frequencies as a function of pressure at the constant temperatures of 252, 275 and 296 K are plotted with the observed ν values [48] in Figs. (3.10-3.12), respectively.

Table 3.9 Raman frequencies calculated as a function of pressure for the Raman modes A_g, A_gB_{2g}, and $B_{1g}B_{3g}$ according to Eq. (3.1) at 252 K for $\gamma_{T(p=0)} = 8.2$, $\gamma_{T(p=0)} = 2.6$ and $\gamma_{T(p=0)} = 3.5$ respectively, in solid benzene.

T=252K	ν_T (cm^{-1})		
P (kbar)	A_g	A_gB_{2g}	$B_{1g}B_{3g}$
1.82	46.76	74.22	120.72
3.51	60.23	80.30	134.53
4.75	72.34	85.02	145.53
5.37	79.23	87.46	151.32

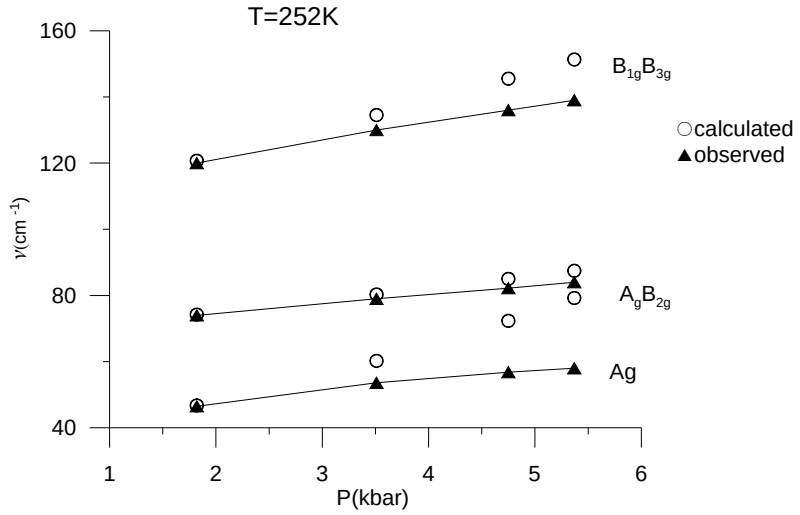

Figure 3.10 Raman frequencies calculated as a function of pressure by using $\gamma_{T(p=0)} = 8.2$, $\gamma_{T(p=0)} = 2.6$ and $\gamma_{T(p=0)} = 3.5$ for the Raman modes A_g, A_gB_{2g}, and $B_{1g}B_{3g}$ respectively according to Eq. (3.1) at 252 K in solid benzene. The observed Raman frequencies are also shown here [48].

Table 3.10 Raman frequencies calculated as a function of pressure for the Raman modes A_g, A_gB_{2g}, and $B_{1g}B_{3g}$ according to Eq. (3.1) at 275 K for $\gamma_{T(p=0)} = 7.6$, $\gamma_{T(p=0)} = 3.4$, and $\gamma_{T(p=0)} = 3.1$ respectively in solid benzene.

T=275K	ν_T (cm^{-1})		
P (kbar)	A_g	A_gB_{2g}	$B_{1g}B_{3g}$
5.54	73.8	87.9	145.0
4.87	67.5	84.4	140.0
3.84	58.8	79.4	132.5
2.1	46.4	71.3	120.5

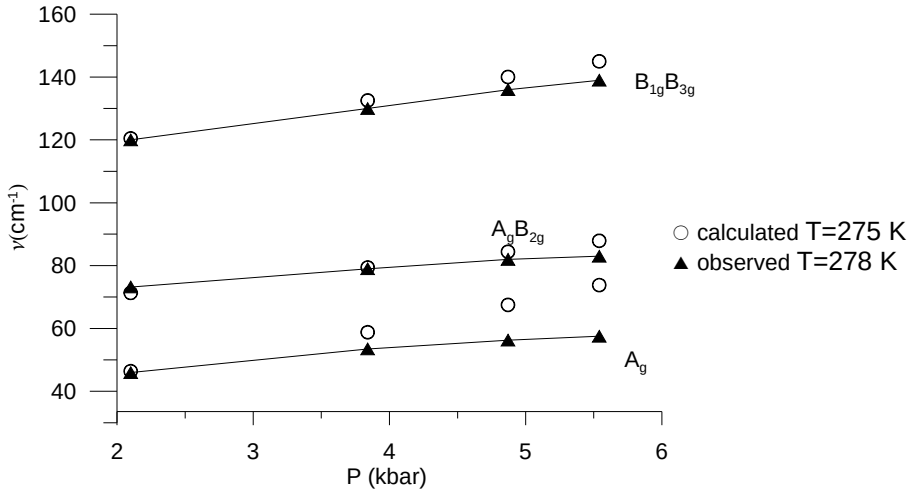

Figure 3.11 Raman frequencies calculated as a function of pressure by using $\gamma_{T(p=0)} = 7.6$, $\gamma_{T(p=0)} = 3.4$ and $\gamma_{T(p=0)} = 3.1$ for the Raman modes A_g, $A_gB_{2g,}$ and $B_{1g}B_{3g}$ respectively according to Eq. (3.1) at 275 K in solid benzene. The observed Raman frequencies at 278 K are also shown here [48].

Table 3.11 Raman frequencies calculated as a function of pressure for the Raman modes A_g, $A_gB_{2g,}$ and $B_{1g}B_{3g}$ according to Eq. (3.1) at 296 K for $\gamma_{T(p=0)} = 9.4$, $\gamma_{T(p=0)} = 3.2$, and $\gamma_{T(p=0)} = 2.2$ respectively in solid benzene.

T=296 K	ν_T (cm^{-1})		
P (kbar)	A_g	A_gB_{2g}	$B_{1g}B_{3g}$
6.525	83.9	91.6	136
5.96	77.7	89.3	133.0
4.71	64.6	83.9	128.0
2.77	46.8	75.3	118.8

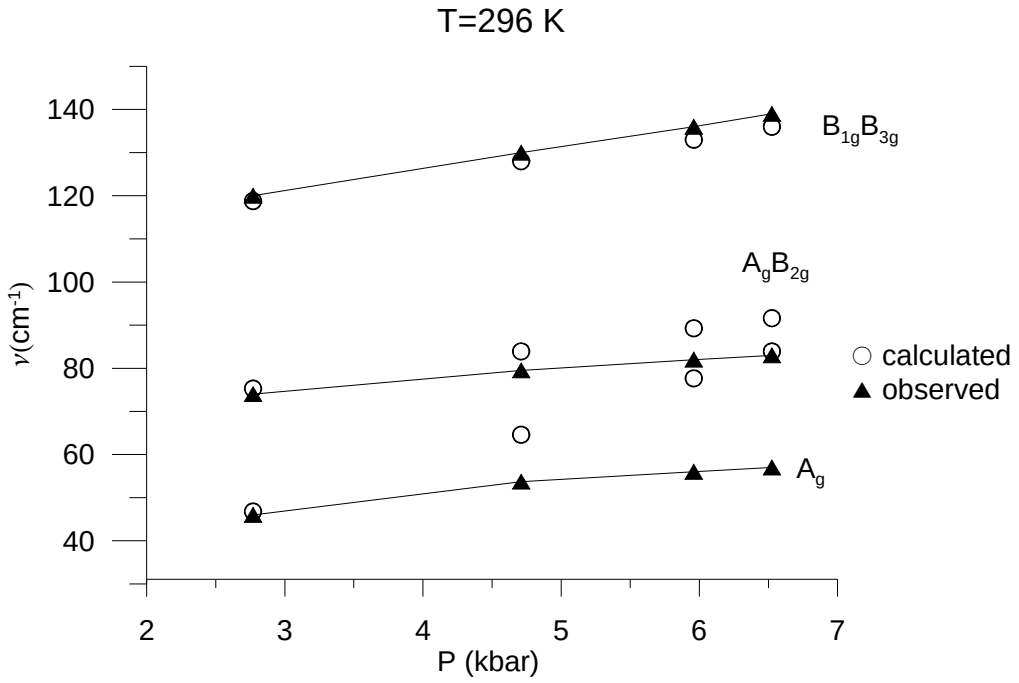

Figure 3.12 Raman frequencies calculated as a function of pressure by using $\gamma_{T(p=0)} = 9.4$., $\gamma_{T(p=0)} = 3.2$ and $\gamma_{T(p=0)} = 2.2$ for the Raman modes A_g, A_gB_{2g}, and $B_{1g}B_{3g}$ respectively according to Eq. (3.1) at 296 K in solid benzene. Observed Raman frequencies are also shown here [48].

This time, we predicted $\nu_T(P)$ from the volume data according to Eq. (3.1) by using the γ_P value at P = 0 for each mode at constant temperatures of 275 and 296 K in the liquid phase of benzene. The results are given in tables 3.12 and 3.13. Raman frequencies as a function of pressure at those temperatures of 275 K and 296 K are plotted in figures 3.13 and 3.14.

Table 3.12 Raman frequencies calculated as a function of pressure by using $\gamma_{T(p=0)} = 7.6$, $\gamma_{T(p=0)} = 3.4$, and $\gamma_{T(p=0)} = 3.1$ for the Raman modes A_g, A_gB_{2g}, and $B_{1g}B_{3g}$ respectively according to Eq. (3.1) at 275 K in liquid benzene.

T=275 K	ν_T (cm^{-1})		
P(kbar)	A_g	A_gB_{2g}	$B_{1g}B_{3g}$
0.36	42.8	68.8	116.7
0.52	45.9	71.0	120.1
0.90	52.0	75.0	126.2
1.18	54.0	76.3	128.1

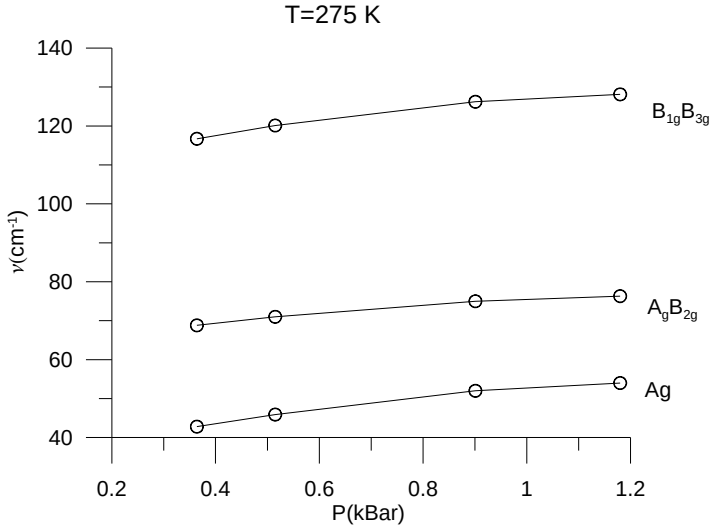

Figure 3.13 Raman frequencies calculated as a function of pressure by using $\gamma_{T(p=0)} = 7.6$, $\gamma_{T(p=0)} = 3.4$, and $\gamma_{T(p=0)} = 3.1$ for the Raman modes A_g, A_gB_{2g}, and $B_{1g}B_{3g}$ respectively according to Eq. (3.1) at 275 K in liquid benzene.

Table 3.13 Raman frequencies calculated as a function of pressure by using $\gamma_{T(p=0)} = 9.4$, $\gamma_{T(p=0)} = 3.2$, and $\gamma_{T(p=0)} = 2.2$ for the Raman modes A_g, A_gB_{2g}, and $B_{1g}B_{3g}$, respectively, according to Eq. (3.1) at 296 K in solid benzene. Values $V_T(p)$ and V_1=$V_m = 83.35\ x10^{-6}\ m^3.mol^{-1}$ are taken from literature [51].

T=296 K		Raman Freq.(cm^{-1})		
$V_T(P)$x10^{-6} ($m^3.mol^{-1}$)	P(MPa)	A_g ($\gamma_{T=9,4}$)	A_gB_{2g} ($\gamma_{T=3,16}$)	$B_{1g}B_{3g}$ ($\gamma_{T=2,18}$)
89.0	26.30	14.9	51.2	91.1
88.0	31.60	16.5	53.1	93.3
87.3	38.70	17.8	54.4	95.0
86.7	42.10	19.0	55.6	96.4
85.6	44.70	21.4	57.9	99.1
85.0	51.30	22.9	59.2	100.7
84.0	57.90	25.6	61.5	103.3
83.3	63.10	27.7	63.1	105.2
82.6	68.40	30.0	64.8	107.1
80.7	71.00	37.3	69.8	112.7
79.0	71.00	45.6	74.6	118.1
74.3	71.00	81.1	90.6	135.0
73.7	84.60	87.5	92.9	137.4

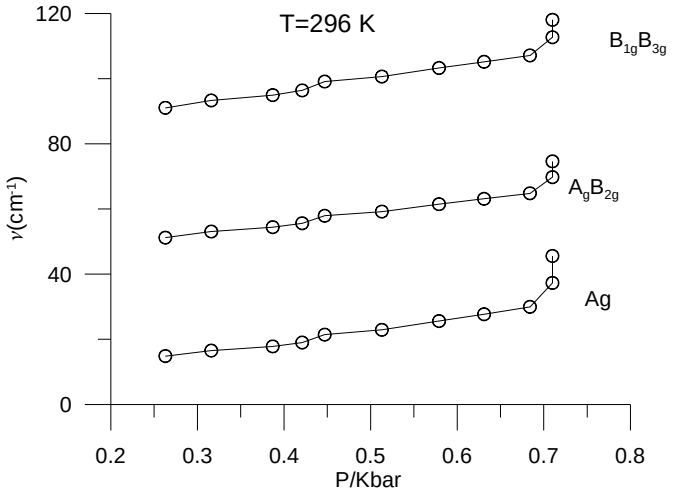

Figure 3.14 Raman frequencies calculated as a function of pressure by using $\gamma_{T(p=0)} = 9.4$, $\gamma_{T(p=0)} = 3.2$, and $\gamma_{T(p=0)} = 2.2$ for the Raman modes A_g, A_gB_{2g}, and $B_{1g}B_{3g}$, respectively, according to Eq. (3.1) at 296 K in liquid benzene.

Finally, we extended our calculations to predict the Raman frequencies by using the volume data for temperatures of 301.5, 313 and 324 K [44, 51]. For this extension, we calculated the γ_T values for the Raman modes A_g, A_gB_{2g}, and $B_{1g}B_{3g}$ at constant temperatures of 301.5, 313 and 324 K. Since there is no corresponding frequency data at these temperatures, we found the extrapolated values of γ_T at constant temperatures of 301.5, 313 and 324 K by using the γ_T values obtained at P=0 for 252, 275 and 296 K.

We determined constants d_0 and d_1 according to a linear fit (Eq. 3.8) by using data in Table 3.8 and the results are given in Table 3.14. By using these coefficients, we calculated the extrapolated values of the mode Grüneisen parameters at constant temperatures of 301.5, 313 and 324 K at zero pressure according to Eq. (3.8) and tabulated in Table 3.14.

$$\gamma_T(P=0) = d_0 + d_1 T \tag{3.8}$$

Table 3.14 Values of the constants d_0 and d_1 (Eq. 3.8) with the extrapolated values of the mode Grüneisen parameter γ_T at P=0 for temperatures 301.5, 313 and 324 K.

Raman modes	d_0	$d_1 x10^{-2}(K^{-1})$	$\gamma_{T=301.5K}$	$\gamma_{T=313K}$	$\gamma_{T=324K}$
A_g	0.97	2.66	9.0	9.3	9.6
A_gB_{2g}	-0.78	1.47	3.7	3.8	4.0
B_1gB_{3g}	11.13	-3.02	2.0	1.7	1.3

Using the γ_T values for each temperature given in Table 3.14, we calculated the Raman frequencies as a function of pressure for the modes A_g, A_gB_{2g}, and $B_{1g}B_{3g}$ according to Eq. (3.1) in the solid and liquid phases. Volume data was taken from literature [51].

Table 3.15 Raman frequencies calculated as a function of pressure for the Raman modes of A_g, A_gB_{2g}, and $B_{1g}B_{3g}$ according to Eq. (3.1) at 301.5 K for $\gamma_{T(=0)} = 9.0$, $\gamma_{T(P=0)} = 3.7$, and $\gamma_{T(P=0)} = 2.0$ respectively in liquid benzene.Values $V_T(P)$ and V_1=$V_m = 82.55\ x\ m^3.mol^{-1}$ are taken from literature [51].

T=301.5 K		ν_P (cm^{-1})		
$V_T(P)$x10^{-6} ($m^3.mol^{-1}$)	P(MPa)	A_g ($\gamma_{T=9.0}$)	A_gB_{2g} ($\gamma_{T=3.7}$)	$B_{1g}B_{3g}$ ($\gamma_{T=2.0}$)
87.2	14.1	14.7	48.8	91.1
86.3	23.6	16.1	50.7	93.1
86.17	35.8	16.3	50.9	95.3
84.6	45.3	19.3	54.5	96.9
84.3	52.8	19.9	55.2	97.6
84.17	57.5	20.2	55.5	97.9
84.00	62.3	20.5	55.9	98.3
83.80	67.9	21.0	56.4	98.8
83.30	72.6	22.1	57.6	100.0
83.00	76.4	22.9	58.4	100.7
82.70	82	23.6	59.2	101.5
81.70	84.9	26.3	61.9	104.0

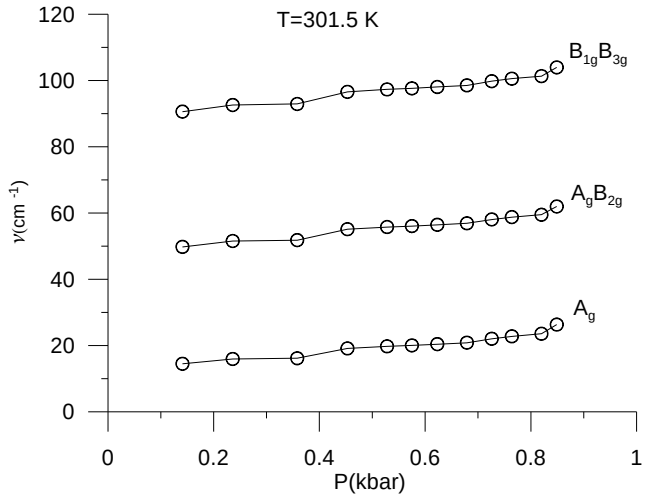

Figure 3.15 Raman frequencies calculated as a function of pressure by using $\gamma_{T(p=0)} = 9.0$, $\gamma_{T(p=0)} = 3.7$ and $\gamma_{T(p=0)} = 2.0$ for the Raman modes A_g, A_gB_{2g}, and $B_{1g}B_{3g}$ respectively according to Eq. (3.1) at 301.5 K in liquid benzene.

Table 3.16 Raman frequencies calculated as a function of pressure for the Raman modes of A_g, A_gB_{2g}, and $B_{1g}B_{3g}$ according to Eq. (3.1) at 313 K for $\gamma_{T(p=0)} = 9.3$, $\gamma_{T(p=0)} = 3.8$, and $\gamma_{T(p=0)} = 1.7$ respectively in liquid benzene.Values $V_T(P)$ and V_1=$V_m = 82.01x10^{-6}\ m^3.mol^{-1}$ were taken from literature [51].

T=313 K		Raman Freq.(cm^{-1})		
$V_T(P)$x10^{-6} $(m^3.mol^{-1})$	P(MPa)	A_g $(\gamma_{T=9,3})$	A_gB_{2g} $(\gamma_{T=3,8})$	$B_{1g}B_{3g}$ $(\gamma_{T=1,7})$
88.75	22.5	15.5	46.7	93.5
88.13	35	16.6	48.0	94.6
87.34	42.5	18.0	49.7	96.1
85.56	53.75	19.5	53.7	99.5
85,50	67.5	21.9	53.9	99.6
84.60	72.5	24.2	56.1	101.4
83.91	85	26.1	58.7	102.8
82.76	96	29.7	61.0	105.2
80.00	106.25	40.7	69.5	111.3
78.90	120	46.2	73.1	114.0
77.96	125	51.7	76.7	116.3
74.38	127.5	80.1	91.8	125.8
74.38	131.25	80.1	91.8	125.8

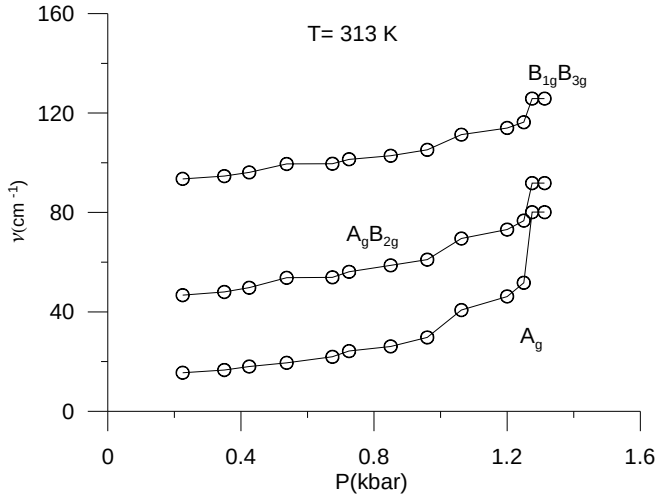

Figure 3.16 Raman frequencies calculated as a function of pressure by using $\gamma_{T(p=0)} = 9.3$, $\gamma_{T(p=0)} = 3.8$ and $\gamma_{T(p=0)} = 1.7$ for the Raman modes A_g, A_gB_{2g}, and $B_{1g}B_{3g}$ respectively according to Eq. (3.1) at 313 K in liquid benzene.

Table 3.15 gives our calculated Raman frequencies of the A_g, $A_gB_{2g,}$ and $B_{1g}B_{3g}$ modes as a function of pressure at a constant temperature of 301.5 K in liquid benzene. Those calculated frequencies are plotted in Fig. 3.15. For T=313K, the pressure dependence of the Raman frequencies calculated (Eq. 3.1) through the values of the mode Grüneisen parameter $\gamma_{T(P=0)}$ (Table 3.14) are given in Table 3.16 and they are plotted in Fig. 3.16.

In order to predict the Raman frequencies of the A_g, $A_gB_{2g,}$ and $B_{1g}B_{3g}$ modes at various pressures for a constant temperature of 328 K in solid benzene, we first determined the values of the mode Grüneisen parameter γ_T for the Raman modes studied here according to Eq. (3.4), as before.

By fitting Eq. (3.3) to the observed Raman frequencies of those modes to the experimental data [48] at 328 K we determined the coefficients b_0, b_1 and b_2; as given in Table 3.17. By using the volume data (Eq. 3.2), the γ_T values for the A_g, $A_gB_{2g,}$ and $B_{1g}B_{3g}$ modes were then determined at a constant pressure of 3.84 kbar (T=328 K) in solid benzene (Table 3.17). Using those γ_T values, the Raman frequencies of those modes were predicted through Eq. (3.1) at T=328 K as a function of pressure, as given in Table 3.18. The Raman frequencies are plotted with the observed data obtained at T=324 K [48] as a function of pressure (T=328 K) in Fig. 3.17.

This time, we predicted the Raman frequencies of A_g, $A_gB_{2g,}$ and $B_{1g}B_{3g}$ modes (Eq. 3.1) by using the pressure dependence of the mode Grüneisen parameter γ_T (P) at T=328 K, as we studied for the other constant temperatures previously. The γ_T values were determined in the pressure range of 3.84 to 7.24 kbar in solid benzene, as tabulated in Table 3.19. Using these γ_T values, the Raman frequencies were evaluated (Eq. 3.1) and they are given in Table 3.19 and are plotted in Fig. 3.18. Our calculated Raman frequencies at 328 K are compared with the observed data at 324 K [48] in this figure. Similar calculation was performed for T=328 K in liquid benzene. For this calculation, the γ_T values at P=0 were first determined for the A_g, $A_gB_{2g,}$ and $B_{1g}B_{3g}$ modes according to Eq. (3.8) using the values d_0, d_1 (Table 3.14) at T=328 K, as given in Table 3.20.

The Raman frequencies of these modes studied were then predicted using Eq. (3.1) where the volume V_T (P) data [51] was used for T=328 K at various pressures in liquid benzene. Our predicted Raman frequencies are given in Table 3.20 and they are plotted as a function of pressure (T=328 K) in Fig. 3.19.

Table 3.17 Values of the coefficients b_0, b_1 and b_2 according to Eq. (3.3) which was fitted in this study to the experimental data [48] for the observed frequencies of the Raman modes indicated at 328 K in the solid benzene. Values of the Grüneisen parameter, γ_T, for the Raman modes obtained from Eq. (3.2) are also given here.

Raman Modes	b_0(cm^{-1})	b_1(cm^{-1}/bar)	b_2(cm^{-1}/bar^2)	γ_T
A_g	32.29	3.55	0.00	4.2
A_gB_{2g}	63.20	2.90	-0.02	12.0
$B_{1g}B_{3g}$	106.80	2.30	-0.05	2.1

Table 3.18 Raman frequencies calculated as a function of pressure for the Raman modes of A_g, $A_gB_{2g,}$ and $B_{1g}B_{3g}$ according to Eq. (3.1) at 328 K for $\gamma_{T(p=3.84)} = 4.2$, $\gamma_{T(p=3.84)} = 2.0$ and $\gamma_{T(p=3.84)} = 2.1$ respectively in solid benzene.

T=328K	ν_T (cm^{-1})		
P (kbar)	A_g	A_gB_{2g}	$B_{1g}B_{3g}$
7.240	57.3	82.8	141.3
6.690	56.0	81. 9	139.7
5.780	53.4	80.1	136.5
3.840	46.9	75.3	128.1

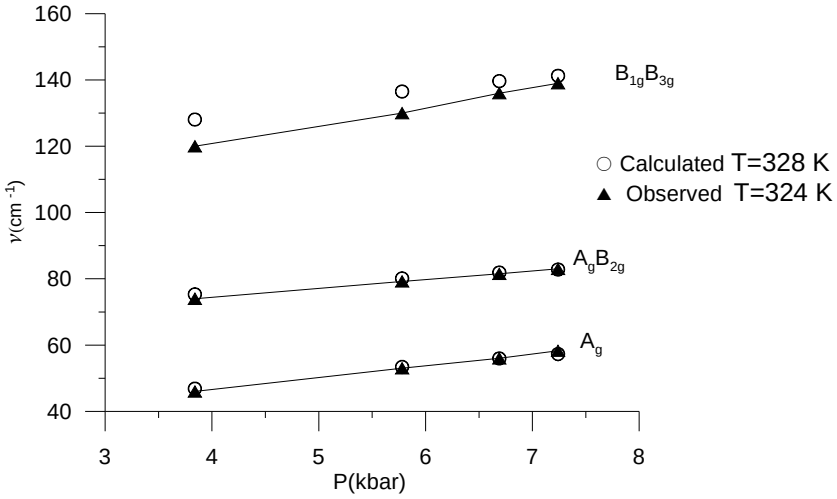

Figure 3.17 Raman frequencies predicted as a function of pressure for the Raman modes A_g, A_gB_{2g}, and $B_{1g}B_{3g}$ according to Eq. (3.1) at 328 K for solid benzene. The observed Raman frequencies at 324 K are also shown here [48].

Table 3.19 Calculated Raman frequencies for the Raman modes A_g, $A_gB_{2g,}$ and $B_{1g}B_{3g}$ according to Eq. (3.1) with mode Grüneisen values at four different pressures for 328 K.

T=328K	**A_g**		**A_gB_{2g}**		**$B_{1g}B_{3g}$**	
P (kbar)	γ_T	$\nu_T(cm^{-1})$	γ_T	$\nu_T(cm^{-1})$	γ_T	$\nu_T(cm^{-1})$
7.240	6.7	80.7	3.3	99.5	5.1	214.2
6.690	6.0	70.4	2.9	92.6	4.2	185.8
5.780	5.1	59.3	2.5	85.0	3.3	158.1
3.840	4.2	46.9	2.0	75.3	2.1	128.1

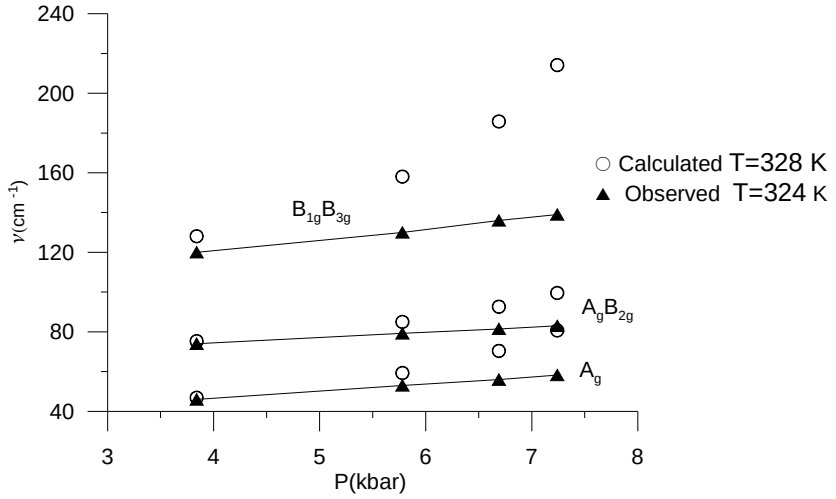

Figure 3.18 Raman frequencies predicted as a function of pressure for the A_g, A_gB_{2g}, and $B_{1g}B_{3g}$ modes according to Eq. (3.1) at 328 K for solid benzene by using the data in Table 3.19. The observed Raman frequencies at 324 K are also shown here [48].

Table 3.20 Raman frequencies calculated as a function of pressure for the Raman modes A_g, A_gB_{2g}, and $B_{1g}B_{3g}$ according to Eq. (3.1) at 328 K for $\gamma_{T(p=0)} = 9.6$, $\gamma_{T(p=0)} = 3.7$, and $\gamma_{T(p=0)} = 1.4$ respectively in liquid benzene.Values $V_T(P)$ and V_1=$V_m = 81.18\, x10^{-6}\, m^3 mol^{-1}$ are taken from literature [51].

T=328 K		Raman Freq.(cm^{-1})		
$V_T(P)$x10^{-6} $(m^3.mol^{-1})$	P(MPa)	A_g ($\gamma_T = 9.6$)	A_gB_{2g} ($\gamma_T = 3.7$)	$B_{1g}B_{3g}$ ($\gamma_T = 1.4$)
86.56	77.50	17.5	48.9	98.0
86.56	80.00	17.5	48.9	98.0
86.10	85.00	18.4	50.0	98.7
85.29	91.25	20.1	51.9	99.9
85.13	96.25	20.5	52.3	100.2
84.53	111.25	21.9	53.8	101.1
83.91	121.25	23.5	55.4	102.2
83.44	136.25	24.8	56.7	102.9
83.13	146.25	25.7	57.5	103.4
82.50	157.50	27.7	59.3	104.5
82.03	163.75	29.2	60.6	105.3
81.72	170.00	30.3	61.6	105.9
81.42	173.75	31.4	62.5	106.4

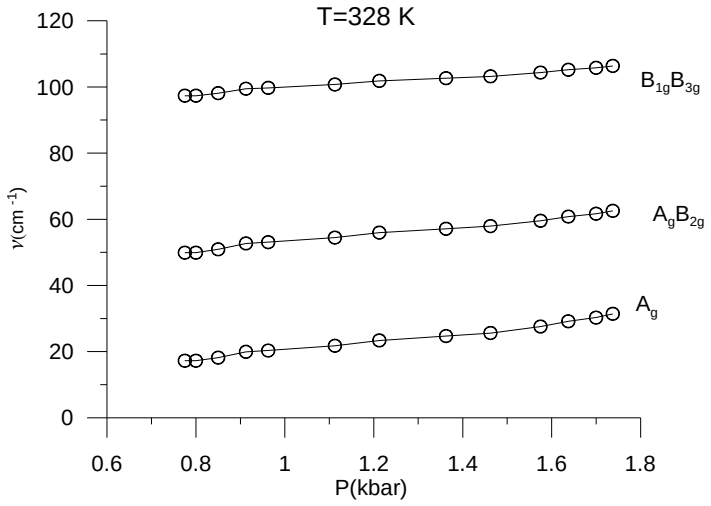

Figure 3.19 Raman frequencies calculated as a function of pressure by using $\gamma_{T(p=0)} = 9.6$, $\gamma_{T(p=0)} = 3.7$ and $\gamma_{T(p=0)} = 1.4$ for the Raman modes A_g, A_gB_{2g}, and $B_{1g}B_{3g}$ respectively according to Eq. (3.1) at 328 K in liquid benzene.

3.3 Discussion

The Raman frequencies for the lattice modes A_g, A_gB_{2g}, and $B_{1g}B_{3g}$ were predicted here as a function of pressure at T = 252 K (Fig. 3.2), T = 278 K (Fig. 3.3) and T = 296 K (Fig. 3.4). By considering the pressure ranges at constant temperatures (for T=252 K, P= 1.82 kbar; for T=278 K, P=2.10 kbar and for T=296 K, P=2.77 kbar) for which the experimental molar volume coefficients were determined, we calculated the mode Grüneisen parameters. The Raman frequencies of the lattice modes considered were predicted using the experimental molar volumes and the Grüneisen parameters determined.

As shown in Figs. 3.2 - 3.4 the Raman frequencies at the temperatures of T=252, 275 and 296 K increase with pressure. As also shown in these figures, our calculated Raman frequencies at constant temperatures of T=252, 275 and 296 K are in good agreement with the observed Raman data for the three lattice modes studied.

We also predicted the Raman frequencies of the the A_g, A_gB_{2g}, and $B_{1g}B_{3g}$ modes as a function of pressure at the same consant temperatures of 252, 275 and

296 K, as shown in Figs. (3.5 – 3.7), respectively by using the mode Grüneisen parameter which was taken as the pressure dependent, $\gamma_T(P)$, with the values given in Table 3.5. Our predicted frequencies (Figs. 3.5 – 3.7) are not any better than those given in Figs. (3.2 – 3.4). In particular, our calculated frequencies of the A_gB_{2g} mode at T=252 K (Fig. 3.5) and $B_{1g}B_{3g}$ mode at 275 K (Fig. 3.6) and $B_{1g}B_{3g}$ mode at T=296 K (Fig. 3.7) agree well with the observed data. For the other lattice modes at constant temperatures, as shown in Figs. (3.5 - 3.7), our calculated frequencies are smaller than those observed values and also they tend to decrease with pressure above about 5 kbar. We also calculated the Raman frequencies using the values of the mode Grüneisen parameter γ_T at zero pressure (P=0) at constant temperatures of 252, 275 and 296 K (Table 3.8), as plotted in Figs. (3.10 – 3.12), respectively. As seen from those figures, agreement between our calculated Raman frequencies and the observed data is good for the A_gB_{2g} mode at constant temperatures of 252 K (Fig. 3.10) and 275 K (Fig. 3.11). For 296 K (Fig. 3.12) our calculated frequencies for this mode deviate above about 5 kbar from the observed data. For the A_g mode, this deviation is considerably large for the three constant temperatures (252, 275 and 296 K). Finally, for the $B_{1g}B_{3g}$ mode agreement between the calculated and observed frequencies is very good for temperatures of 275 K (Fig. 3.11) and 296 K (Fig. 3.12), whereas for T=252 K (Fig. 3.10) our calculated frequencies get larger than those observed values above 5 kbar. From these treatments, we conclude that a costant mode Grüneisen parameter for each mode at the temperatures of 252, 275 and 296 K (Table 3.3) provides the Raman frequencies calculated as a function of pressure, which agree very well with the observed data in solid benzene (Figs. 3.2 – 3.4).

For the liquid benzene, the Raman frequencies of the three lattice modes (A_g, A_gB_{2g}, and $B_{1g}B_{3g}$) were predicted at constant temperatures of 275 K (Fig. 3. 8) and 296 K (Fig. 3.9) by using constant mode Grüneisen parameter for each mode at P=2.1 and P=2.77 kbar, respectively,(Table 3.3) as stated above. As we see from both figures (Figs. 3.8 and 3.9), the Raman frequencies predicted for the three modes increase with pressure in the liquid phase, as in the solid phase. At T= 296 K (Fig. 3.9) there occurs a phase transformation at around 71 MPa (0.71 kbar),

whereas there is no anomalous behavior at the temperature of 275 K (Fig. 3.8). Anomaly in the Raman frequency is exhibited at 296 K by the three lattice modes (the A_g, A_gB_{2g}, and $B_{1g}B_{3g}$) as shown in Fig. 3.9.

The Raman frequencies of those lattice modes were also predicted using the γ_P values at P=0 (Table 3.12) in liquid benzene for the temperatures of 275 K (Fig. 3.13) and 296 K (Fig. 3.14). Since the values of the Grüneisen parameter for each mode are higher at P=0 (Table 3.12) then those at a constant pressure of P=2.1 kbar (T=275 K), the Raman frequencies predicted (Fig. 3.13) are higher than those predicted (Fig. 3.8). For a constant temperature of 296 K, an anomalous behavior of the frequency for three modes is also exhibited when the Raman frequencies were calculated using the γ_T(P=0) values as a function of pressure (Fig. 3.14), as in Fig. (3.9) in liquid benzene.

We have extended our calculation of the Raman frequencies for the lattice modes of A_g, A_gB_{2g}, and $B_{1g}B_{3g}$ at T=301.5 K (Fig. 3.15) and 313K (Fig. 3.16) in liquid benzene as a function of pressure. There is an indication that the Raman frequency ν of the A_g and A_gB_{2g} modes increases considerably, whereas there is no anomaly for the the $B_{1g}B_{3g}$ mode at T=313 K as shown in Fig. 3.15 (T=301.5 K). Similarly, we extended our calculation of the Raman frequencies for the A_g, A_gB_{2g}, and $B_{1g}B_{3g}$ modes as a function of pressure for T=328 K (Fig. 3.17) by using the γ_T values (Table 3.18) and also using the γ_T values (Table 3.19), as shown in Fig. 3.18 in solid benzene. When compared with the observed data at T=324 K, our predictions agree very well with the observed data when a constant γ_T value for each mode was used (Table 3.18), as shown in Fig. 3.17. Our calculated ν values are much higher than those obtained experimentally (Fig. 3.18). In particular, our predicted ν values for the $B_{1g}B_{3g}$ deviate largely above 5 kbar when compared with the observed data (Fig. 3.18). Similarly, the Raman frequencies of the A_g, A_gB_{2g}, and $B_{1g}B_{3g}$ modes were predicted as a function of pressure for T=328 K in liquid benzene (Fig. 3.19) by using the γ_T values at P=0 (Table 3.20). As shown in Fig. 3.19, our calculated frequencies increase with pressure (T=328 K), which can be compared with the observed data when available in literature.

As shown in these figures (3.2 - 3.19), variation of the Raman frequencies with the pressure at constant temperatures is nonlinear in the solid and liquid benzene. This behavior is related to the large initial compressibility of benzene, which can occur in most of the molecular crystals. This pressure dependence of the Raman frequencies gives rise to the mode Grüneisen parameter which measures anharmonicity of a molecular crystalline system. For benzene, we determined the values of the Grüneisen parameters for the A_g, A_gB_{2g}, and $B_{1g}B_{3g}$ modes, which vary from 2.3 to 5.9 (Table 3.3) and also $\gamma_T(P)$ values which vary from 1.0 to 5.9 for the three modes as the pressure decreases from about 6 to 2 kbar (Table 3.5). We also obtained the γ_T values at P=0 for the A_g, A_gB_{2g}, and $B_{1g}B_{3g}$ modes, which vary from 2 to 9 for constant temperatures of 252, 275 and 296 K (Table 3.8). At higher temperatures of 301.5, 313 and 324 K we determined the γ_T values at P=0 as about 9.5 (A_g mode), 4 (A_gB_{2g}, mode) and 2 ($B_{1g}B_{3g}$ mode), as given in Table 3.14. In particular for T=328 K, the γ_P values at P=3.84 kbar where 4.2, 2.0 and 2.1 for the A_g, A_gB_{2g}, and $B_{1g}B_{3g}$ modes, respectively (Table 3.18).

Our values determined here for the mode Grüneisen parameter γ_T of the A_g, A_gB_{2g}, and $B_{1g}B_{3g}$ modes can be compared with those of γ_{ext} (external or lattice modes) which vary between 2.5 and 3.1 in the orthorhombic phase I and the values between 1.8 and 3.1 in the monoclinic phases II and III of benzene [55]. It has also been found that the Grüneisen parameters have the same values when they are calculated from the Raman frequencies measured as a function of temperature at constant pressures within the experimental uncertainties, in particular for phase I of benzene [55].

Finally, this increase in the Raman frequency of the lattice modes with increasing pressure (Figs. 3.2 – 3.8, 3.10 – 3.12, 3.17, 3.18) which we obtained in this study, increases the ordering in the solid benzene. This gives rise to a decreasing entropy and a decreasing linewidth of the Raman modes, as also pointed out previously for solid benzene I [42].

CHAPTER 4

CONCLUSIONS

In this study we have calculated the temperature and pressure dependence of the Raman frequencies of nitrogen and benzene for some lattice in the solid phases and modes close to the melting line. To perform this calculation, we used the volume data from the literature through the mode Grüneisen parameter.

In chapter 2, the temperature and pressure dependence of the Raman frequencies for the lattice modes were calculated by using the observed data for the molar volume in the β phase and also on the melting curve between the solid β phase and the fluid phase in nitrogen. This calculation was performed by considering a constant mode Grüneisen parameter for each lattice mode throughout the β phase and the melting line in solid nitrogen.

In chapter 3, experimental molar volume data was used to calculate the pressure dependence of the Raman frequencies for the lattice modes A_g, $A_gB_{2g,}$ and $B_{1g}B_{3g}$ in solid and liquid benzene. To perform this calculation, the values of the Grüneisen parameter was calculated for each lattice mode as in the solid nitrogen.

To conclude, our calculated Raman frequencies are in good agreement with the observed Raman data in the β phase and also close to the melting line in solid nitrogen. Also, the calculated Raman frequencies of benzene are reasonable compared with the observed Raman data. These results show that the method of calculating the Raman frequencies from the volume data is satisfactory and that it can be applied to some other molecular crystals such as solid nitrogen and benzene.

REFERENCES

[1] H. Eugene Stanley, Introduction to Phase Transitions and Critical Phenomena, Clarendon Press Oxford (1971).

[2] A. B. Pippard, Elements of Classical Thermodynamics for Advanced Students of Physics, Cambridge at the University Press (1966).

[3] Hidetoshi Nishimori, Gerardo Ortiz, Elements of Phase Transitions and Critical Phenomena, Oxford University Press (2011).

[4] Victor A. Shashilov, Development of Mathematical Methods for Quantitativ Resonance Raman Spectroscopy, ProQuest (2007).

[5] M. M. Sushchinskiy, Inelastic Light Scattering in Crystals, Nova Publishers (1989).

[6] F. D. Medina and W. B. Daniels, J. Chem. Phys. 64 (976) 150.

[7] S. Buchsbaum, R. L. Mills and D. Schiferl, J. Phys. Chem. 88 (1984)2522.

[8] H. Schneider, W. Häfner, A. Wokaun and H. Olijnyk, J. Chem. Phys. 96 (1992) 8046.

[9] E. Gregoryanz, A. F. Goncharov, R. J. Hemley, H. K. Mao, M. Somayazulu and G. Shen, Phys. Rev. B66 (2002) 224108

[10] J. A. Venables and C. A. English, Acta Cryst Sect. B 30 (1974) 929.

[11] W. E. Streib,T. H. Jordan and W. N. Lipscomb, J. Chem. Phys. 37 (1962) 2962.

[12] R. L. Mills and A. F. Schuch, Pyhs. Rev. Lett. 23 (1969) 1154.

[13] J. Felsteiner, D. B. Litvin and J. Zak, Phys. Rev. B. 3 (1971) 2706.

[14] D. T. Cromer, R. L. Mills, D. Schiferl and L. A. Schwalbe, Acta Cryst. Sect. B 37 (1981) 8.

[15] T. Westerhoff, A. Wittig and R. Feile, Phys. Rev. B 54 (1996) 14.

[16] D. C. Heberlein, E. D. Adams and T. A. Scott, J. Low Temp. Phys. 2 (1970) 449.

[17] V. G. Manzhelii, A. M. Tolkachev and E, I, Voitovich, Phys. Stat. Sol. 13 (1966) 351.

[18] M. I. Bagatskii, V. A. Kutcheryavy, M. G. Manzelii and V. A. Popov, Phys. Stat. Sol. 26 (1968) 453.

[19] H. Olijnyk, J. Chem. Phys. 93 (1992) 8968.

[20] A. Anderson, T. S. Sun and M. C. A. Donkersloot, Can. J. Phys. 48 (1970) 2265.

[21] P. M. Mathai and E. J. Allin, Can. J. Phys. 49 (1971) 1973.

[22] A. F. Goncharov, E. Gregoryanz, H. K. Mao and R. J. Hemley, Low Temp. Phys. 27 (2001) 866.

[23] L. Tassini, F. Gorelli and L. Ulivi, J. Chem. Phys. 122 (2005) 074701.

[24] E. Gregoryanz, A. F. Goncharov, R. J. Hemley and H. K. Mao, J. Chem. Phys. 126 (2007) 184505.

[25] R. Caracas, J. Chem. Phys. 127 (2007) 144510.

[26] T. S. Kuan, A. Warshel and O. Schnepp, J. Chem. Phys. 52 (1970) 3012.

[27] T. Luty and G. S. Pawley, Chem. Phys. Lett. 28 (1974) 593.

[28] J. P. Michels, M. E. Kooi and J. A. Schouten, J. Chem. Phys. 108 (1998) 2695.

[29] M. Ross and F. Rogers, Phys. Rev. B74 (2006) 024 103.

[30] I. Kotakoski and K. Albe, Phys. Rev. B 77 (2008) 144109.

[31] B. Boates and S. A. Bonev, Phys. Rev. Lett. 102 (2009) 015701.

[32] Y. Ma, A. R. Oganov, Z. Li, Y. Xie and J. Kotakoski, Pyhs. Rev. Lett. 102 (2009) 065501.

[33] H. Yurtseven and T. Tunay, Int. J. Mod. Phys. B 24 (2010) 6069.

[34] M. Kurt and H. Yurtseven, Int. J. Mod. Phys. B (in press) 2011.

[35] M. I. M. Scheerboom and J. A. Schouten, J. Chem. Phys. 105 (1996) 2553.

[36] R. Bini, L. Ulivi, J. Kreutz and H. J. Jodl, J. Chem. Phys. 112 (2000) 8522.

[37] A. F. Schuch and R. L. Mills, J. Chem. Phys. 52 (1970) 6000.

[38] R. L. Mills, B. Ollinger and D. T. Cromer, J. Chem. Phys. 84 (1986) 2837.

[39] W. D. Ellenson and M. Nicol, J. Chem. Phys. 61 (1974) 1380.

[40] P. W. Bridgman, J. Chem. Phys. 9 (1941) 794.

[41] M. M. Thiery, D. Fabre, I. Spain and K. Kobashi, Physica B 139-140 (1986) 520.

[42] F. Cansell, D. Fabre and J. P. Petitet, J. Chem. Phys. 99 (1993) 7300.

[43] L. Ciabini, F. A. Gorelli, M. Sentoro, R. Bini, V. Schettino and M Mezouar, Phys.Rev. B 72 (2005) 094108.

[44] P. Figuirè, A. H. Fuchs, M. Ghelfenstein and H. Szwarc, J. Phys. Chem. Solids 39 (1978) 19.

[45] Ph. Pruzan, D.H. Liebenberg and R.L. Mills, J. Phys. Chem. Solids 47 (1986) 949.

[46] P. W. Bridgman, The Physics of High Pressure, London: G. Bell and Sons, Ltd. 1931.

[47] G. G. Dumas, Spectrochimica Acta 30A (1974) 1623.

[48] M. Ghelfenstein and H. Szwarc, Chem. Phys. Lett. 32 (1975) 93.

[49] M. Gehrig and H Lentz, J. Chem. Thermodynamics, 9 (1977) 445.

[50] H Yurtseven and T. Ünsal, High Temp. Mater Processes 26 (2007) 365.

[51] H Yurtseven and T. Ünsal, Tsinghua Science and Technology 12 (2007) 624.

[52] H. Yurtseven, B. Raşitoğlu and E. Kilit, J. Mol. Struc. 993 (2011) 428.

[53] S. Block, C. E. Weir and G. J. Piermarini, Science 169 (1970) 586.

[54] J. Akella and G. C. Kennedy, J. Chem. Phys. 55 (1971) 793.

[55] M. M. Thiery and J. M. Leger, J. Chem. Phys. 89 (1988) 4255.